REPORT NO. FAA-RD-74-46

AIRBORNE WAKE VORTEX DETECTION

J. D. Fridman

MARCH 1974

FINAL REPORT

DOCUMENT IS AVAILABLE TO THE PUBLIC THROUGH THE NATIONAL TECHNICAL INFORMATION SERVICE, SPRINGFIELD, VIRGINIA 22151.

Prepared for

DEPARTMENT OF TRANSPORTATION
FEDERAL AVIATION ADMINISTRATION
Systems Research and Development Service
Washington DC 20590

Technical Report Documentation Page

1. Report No.	2. Government Accession No.	3. Recipient's Catalog No.
FAA-RD-74-46		

4. Title and Subtitle	5. Report Date
AIRBORNE WAKE VORTEX DETECTION	March 1974
	6. Performing Organization Code
	8. Performing Organization Report No.
7. Author(s)	DOT-TSC-FAA-74-3
J. D. Fridman*	
9. Performing Organization Name and Address	10. Work Unit No. (TRAIS)
Raytheon Company Equipment Development Laboratories Sudbury MA 01776	R-4115/FA405
	11. Contract or Grant No.
	DOT-TSC-522
	13. Type of Report and Period Covered
12. Sponsoring Agency Name and Address	Final Report Sept. 1972-March 1973
Department of Transportation Federal Aviation Administration Systems Research and Development Service Washington DC 20590	14. Sponsoring Agency Code

15. Supplementary Notes

*Under contract to: Department of Transportation
Transportation Systems Center
Kendall Square
Cambridge MA 02142

16. Abstract

Active and passive remote sensing systems were assessed to determine the feasibility of detecting aircraft trailing vortices using instrumentation on-board an aircraft. It was found that a modification of the front-end receiver of a 10 GHz weather radar system or a change of frequency to 35 GHz may allow vortex identification over a range of several kilometers. The CO_2 laser coherent Doppler radar technique and passive radiometric techniques (8-14 microns) show considerable promise. Other airborne systems (incoherent Lidar, Raman shift techniques, fluorescence scattering, acoustic radar, ultraviolet emissions) were shown not to possess sufficient sensitivity.

17. Key Words	18. Distribution Statement
. Wake Vortices . Lidar . Weather Radar . IR	DOCUMENT IS AVAILABLE TO THE PUBLIC THROUGH THE NATIONAL TECHNICAL INFORMATION SERVICE, SPRINGFIELD, VIRGINIA 22151.

19. Security Classif. (of this report)	20. Security Classif. (of this page)	21. No. of Pages	22. Price
Unclassified	Unclassified	92	

Form DOT F 1700.7 (8-72) Reproduction of completed page authorized

PREFACE

This study was performed under Contract No. DOT-TSC-522 for the Department of Transportation, Transportation Systems Center, Cambridge, Mass. The author would like to thank Dr. James Hallock, Technical Monitor, DOT/TSC for his sponsorship of this work, guidance and continuing interest in the results of this study. Many discussions held with a number of individuals, from many interested organizations, have helped bring forth current opinion and state-of-the-art progress in the special areas covered by this report. In particular, thanks are due to:

Dr. Robert Muñoz, NASA Ames Research Center, Moffett Field, Cal.

Dr. K. M. Glover, Air Force Cambridge Research Center, Bedford, Mass.

Mr. Jack Grobman, NASA Lewis Research Center, Cleveland, Ohio

Mr. W. D. Wood, DOT/TSC

Mr. Donald A. Leonard, Avco-Everett Research Laboratory, Everett, Mass.

Mr. D.A. Kawachi, Electro Optics Dept., Raytheon Co., Sudbury, Mass.

Dr. V. E. Derr, NOAA, Boulder, Colorado

Dr. Sheila Widnall, MIT, Cambridge, Mass.

Mr. George Michanowsky, Amazonia Foundation, New York, N. Y.

Mr. Albert V. Jelalian, Electro-Optics Department, Raytheon Company, Sudbury, Mass.

Mr. Roger W. Goff, Electro-Optics Department, Raytheon Company, Sudbury, Mass.

Mr. William Keil, Delta Airlines, Boston, Mass.

for their contributions.

TABLE OF CONTENTS

TABLE OF CONTENTS (continued)

LIST OF ILLUSTRATIONS

LIST OF ILLUSTRATIONS (continued)

SECTION 1

INTRODUCTION

1.1 DEFINITION OF PROBLEM

The introduction of large transport aircraft, the B-747, L-1011, DC-10; the increasing utilization of airports to capacity by the use of the now conventional B-707, B-727, and DC-8 aircraft; and the increase in the general aviation traffic has given to the wake vortex problem from an airport safety and flight economics point-of-view, added scope and significance. The vortices generated by large aircraft can create dangerous encounter situations with other airplanes as a result of their slow dissipation rates or in conjunction with unfavorable meteorological conditions that prolong their presence over a runway. An interaction occurring in the terminal area and approach corridors of airports, at arrival or departure, may generate roll moments exceeding the roll stability of the vortex encountering aircraft with the resultant hazardous situation leading to roll-over, loss of altitude and ultimate destruction.

In order to forestall such events and to control the time between landings, thus at the same time increasing the air traffic handling capability of an airport, ground-based instrumentation systems located near the middle marker are under development. Such instrumentation may consist of the following sensors that have been shown to detect, track and identify ground wind and trailing vortex structures. They are:[1]

a) propeller anemometers
b) pulse acoustic radar
c) CW Doppler acoustic radar
d) monostatic acoustic radar
e) laser Doppler radar

1.2 AIRBORNE VORTEX DETECTION SYSTEMS NEEDS

While the potential use of such ground-based instrumentation systems gives the air traffic controllers responsibility to assess the presence or absence of an undesirable vortex and thus notify the pilot of its presence, it does not permit the pilot to assess the impending presence of the vortex when the plane lands under VFR (Visual Flight Regulations) conditions. Until the pilot approaches the mid-marker area that may be surveyed by the ground-based vortex instrumentation system, he does not know of the presence, intensity, distance to and time duration of vortex pairs generated by the airplane preceeding his during the landing phase. Hence, whether the pilot is on VFR or IFR (Instrument Flight Regulations) an independent assessment, by his own means, of the vortex location in his flight of path would promote: a) safety b) concrete knowledge of the vortex presence c) better use of the available air space. The pilot can thus help out the aircraft queuing problem by moving in closer to or increasing his distance from the aircraft ahead of him. During takeoff, determining the presence of a vortex pair on his own will save him from running into any, a common occurrence, thus contributing to the overall comfort and safety of his passengers and airplane.

1.3 AIRBORNE VORTEX DETECTION SYSTEM REQUIREMENTS

Figure 1-1 is a pictorial representation of the airport and airplane vortex measurement requirements. Figure 1-2 is a schematic of the airport landing envelope, as defined by present standards. An in-flight vortex measurement system must operate over a range of about

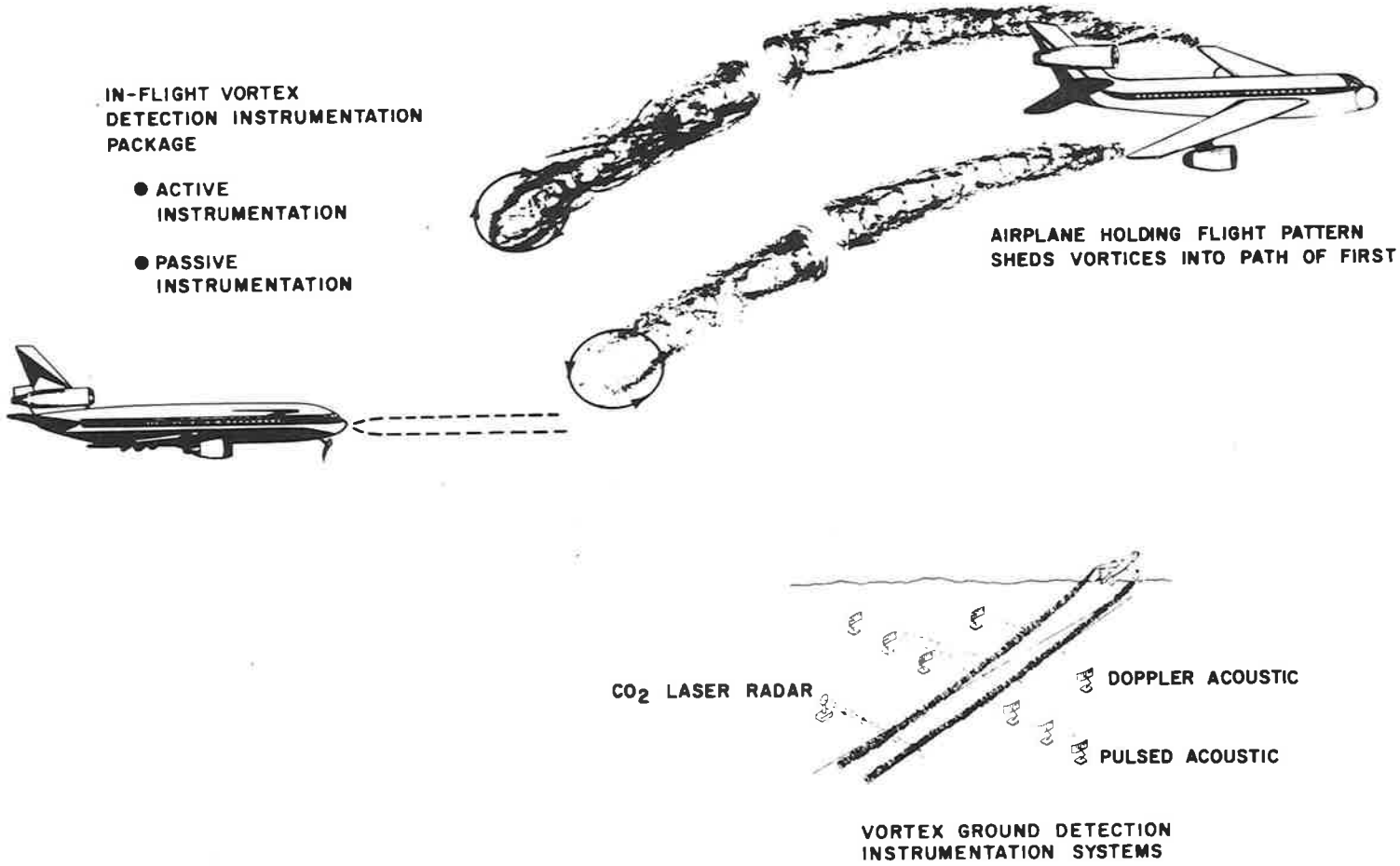

Figure 1-1. IN-FLIGHT DETECTION OF VORTICES

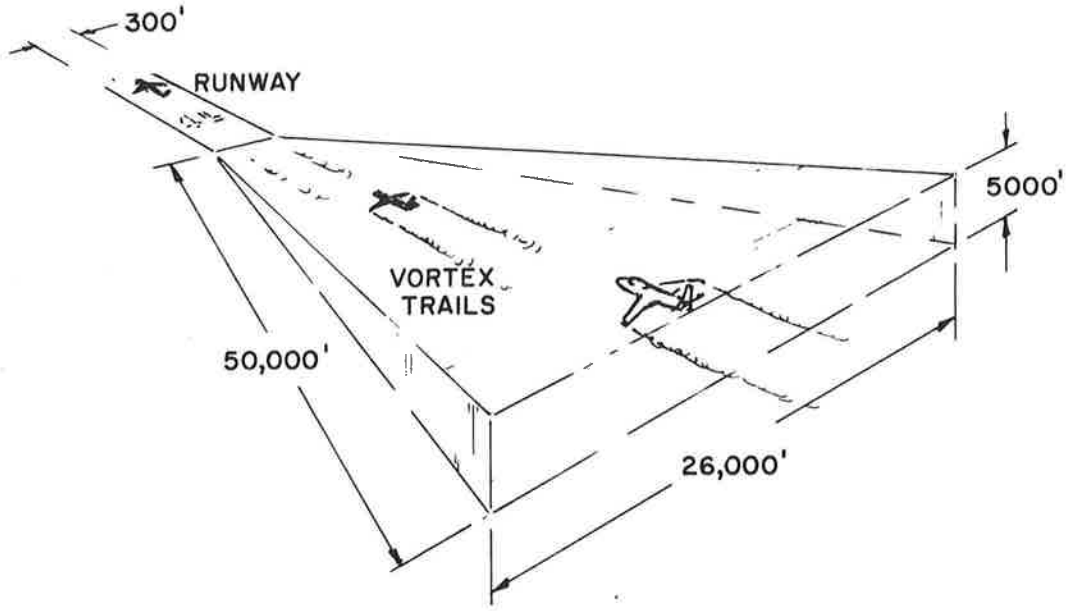

Figure 1-2. Airborne Vortex Detection System

SPECIFICATIONS

- MINIMUM DETECTION SENSITIVITY: 0.5 MILES
- MAXIMUM DETECTION SENSITIVITY: 5 TO 10 MILES
- ALL WEATHER CAPABILITY: IF NOT ACHIEVABLE, LIMITATIONS OF SYSTEM SHOULD BE PREDICTABLE
- SENSORS MUST HAVE A DIRECTIVITY ENHANCED BY A SCANNER
- OPERATIONAL ALTITUDE: TO 5000 FEET

five miles to be useful in the context of the airborne system previously described. It must also be operable over shorter distances, down to a distance of 0.5 miles, under acceptable weather conditions. Altitude of operation is from 500 feet to 1200 feet with capabilities to perform such measurements up to an altitude of five kilofeet. The instrumentation that one would ideally like to use must be inexpensive, emphasis being on modifications of any presently on-board remote sensing systems. If such a condition cannot be satisfied, such instrumentation must still conform to norms of simplicity, accuracy, reliability, low cost and versatility.

This study has been undertaken with the purpose of assessing the performance of active and passive remote sensing instrumentation systems that may be potential candidates for such an airborne vortex detection system. They have been defined in terms of their predictive characteristics to identify the presence of a vortex trail by its physical signatures. Hence, a definition of what such signatures are and how they develop, information that is presently not well defined or known, has been necessary in order to then assess possible instrumentation candidates. Section 2 is a brief presentation of the known physical parameters of the vortex. Section 3 is an analysis of active and passive microwave, optical, acoustic and spectroscopic systems that bear upon a set of choices, as concluded in Section 4, available for application to this problem.

SECTION 1 - REFERENCES

(1) Wood, W. D., Hallock, J. N., Spitzer, E. A.; "Wake Vortex Program", Transportation Conference, NEREM '73, November 6, 1973, Boston, Mass.

SECTION 2

CHARACTERISTICS OF TRAILING VORTICES

2.1 PHYSICAL FEATURES

In order to assess the feasibility of applying active and passive remote sensing instrumentation systems, as for instance microwave, optical and acoustic radars or spectroscopic and radiometric techniques to the detection of aircraft trailing vortices, it is essential to define, as accurately as possible, the physical characteristics of such vortices. These physical characteristics may encompass all fluid mechanical processes, engine emissions, and spectroscopic characteristics of the wake that may directly or indirectly, through their interaction with the ambient atmosphere, generate the necessary signatures that identify the presence of the vortex. These processes, however, are at the present time not completely defined and the transport characteristics that they possess in relationship to the ambient atmosphere have not always been substantiated through experimental measurements. Thus, by defining as much that is known about the behavior of the vortex wake and its accompanying effects on the ambient atmosphere and extrapolating theoretically beyond the experimental evidence, we will arrive at possible models which will be used to evaluate remote sensing instrumentation systems.

The wake behind the aircraft may be subdivided into the jet, vortex and dispersion regimes, corresponding to observed behavior. Figure 2-1 are photographs[1] generated by a B-52 aircraft of a typical exhaust trail. Figure 2-2 shows the contrail dimensions as a function of time and regime classification. The jet regime extends from the engines to the point where the jets occupy all the recirculating region associated with the trailing vortex pair (indicated as

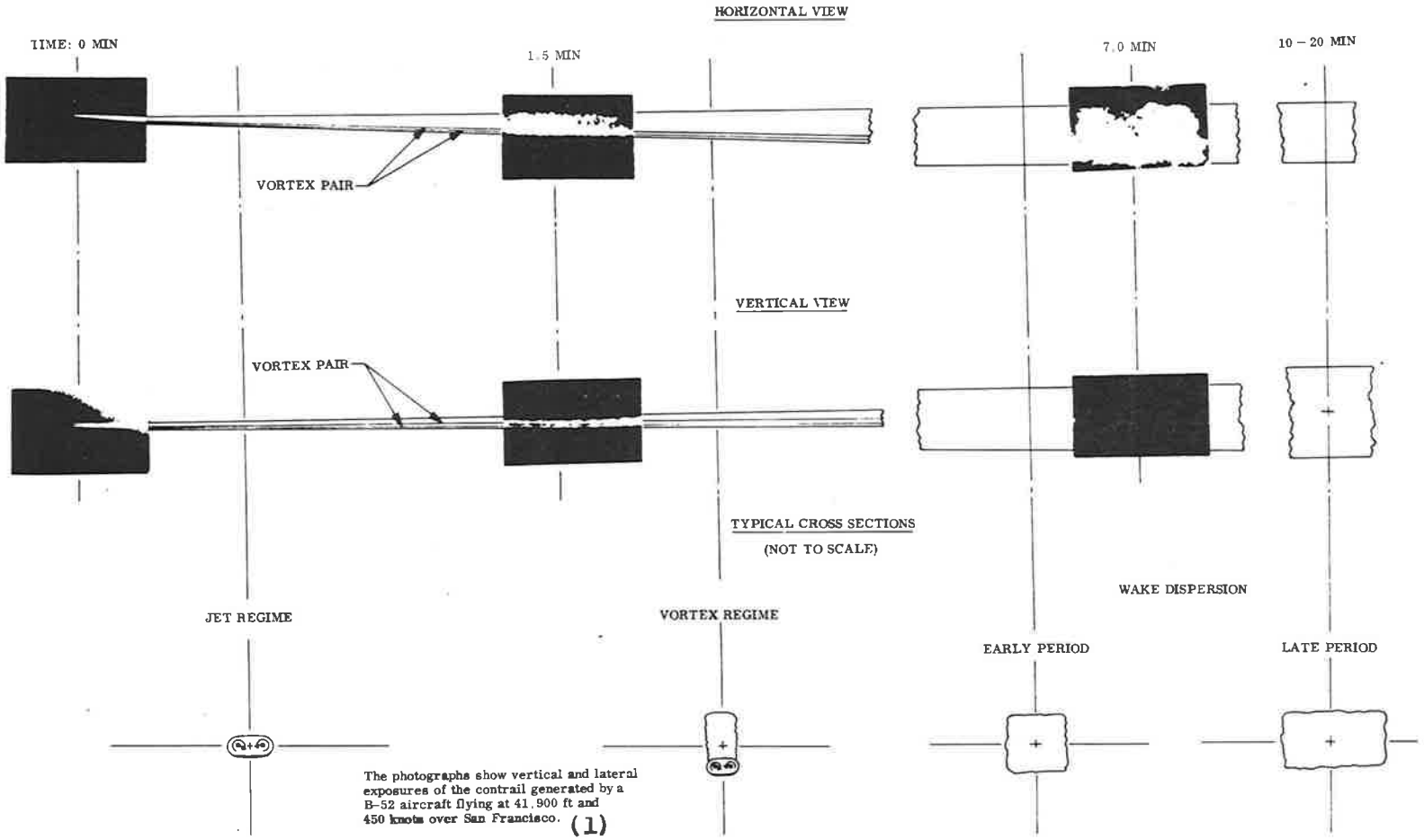

Figure 2-1. Typical Exhaust Trail

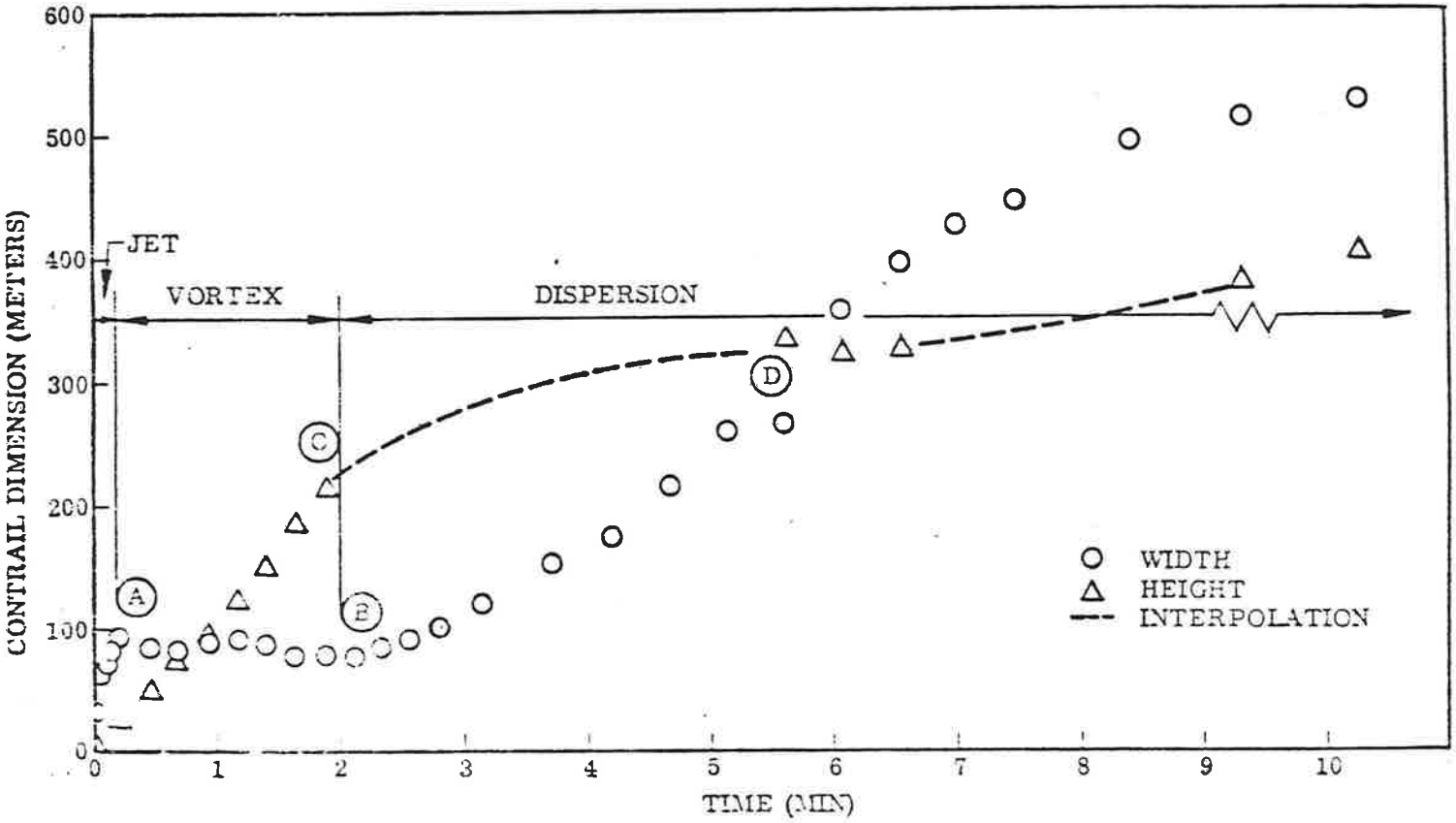

Figure 2-2. Time History of B-52 Exhaust Trail Shown in Figure 2-1.

Point A in Figure 2-2). This corresponds to a time on the order of 10 sec and a distance on the order of 2 km. In this region the exhaust trail initially occupies only a fraction of the overall aircraft wake since it is confined to the turbulent jets issuing from the engines. Eventually, these jets become immersed in the developing vortex field and are attracted to the cores because of jet buoyancy. The details of jet-vortex interaction and appearance of the exhaust trail are dependent on the detailed aircraft configuration, such as number and placement of the engines. The vortex regime extends from the end of the jet regime to the point where the vortex pair breaks up because of hydrodynamic instability. This regime lasts for times of the order of 100 sec and extends over distances on the order of 20 km along the flight path. The unusual feature of this regime--namely, vertical growth with little or no horizontal growth--can be explained by the fact that the wake in this regime is dominated by the trailing vortex pair. The exhaust gases, which originally fill the recirculating flow associated with the sinking vortex pair, become detrained from the pair and are deposited in a region of roughly rectangular cross-section, with the top at the original flight level and the bottom at the vortex pair. Thus, the vortex pair restrains the exhaust from horizontal growth and promotes vertical growth instead. The upper central photograph in Figure 2-1 shows the cores of the sinking vortex pair and the detrained exhaust above them. This effect, which is induced entirely by the aircraft, has a lasting impact on the wake because the vertical growth exposes it to wind shear, which is one of the major mechanisms for further dispersal in the wake dispersion regime.

In the vortex regime, atmospheric environment again plays a secondary role. The characteristics of the vortex pair, such as circulation strength, pair separation distance, time-to-vortex sheet roll-up, and sinking rate are principally related to the aircraft and

flight characteristics. Some of the more important parameters are aircraft weight, flight velocity, lift distribution, and wing span. Given the aircraft and flight characteristics, the major features of the vortex pair can be predicted. Table 2-I is a classification of such characteristics.

The wake-dispersion regime lasts from vortex breakup to a time on the order of 1,000 sec, during which the exhaust changes from an aircraft-dominated condition to a mode of natural atmospheric dispersal.

2.2 WAKE VORTEX VELOCITY DISTRIBUTIONS

Table 2-I is a compilation of some commercial aircraft characteristics and their measured or calculated vortex properties.

Maximum tangential velocities have been measured, as shown, on tower fly-byes, on a number of aircraft. These values are realistic and have been used in the calculation of the vortex core boundary diameter, using the simplified line-vortex model, where:

$$v_\theta = \frac{\Gamma}{\pi D} \qquad (2\text{-}1)$$

where: v_θ = maximum tangential velocity
Γ = vortex circulation
D = core boundary diameter

The vortex rate of descent for the B-707 and B-747 has been calculated by the formula:

$$\frac{dz}{dt} = -\frac{4}{\pi^2} v_o \frac{C_L}{\pi A} \qquad (2\text{-}2)$$

Table 2-I. Aircraft and Vortex Characteristics

AIRCRAFT CHARACTERISTICS								VORTEX CHARACTERISTICS				
Aircraft	Engine Location and Number/ Wing	Weight Lbs.	Wing Span Ft.	Area $Ft.^2$	Aspect Ratio	Take-off Speed MPH	Landing Speed MPH	Γ Vortex Strength $Ft.^2/sec$	Vortex Diameter Ft.	V_θ Tangential Velocity Ft./sec	Vortex Rate of Descent[c] Ft./sec	Vortex Age
B-707	Wings 2	258,000	145.75	2892	7.36	195	157	4165	10.0[s]	132.4	5.4[(1)]	Vortex may break up on runway within 2 minutes. May last up to 5 minutes in atmosphere. Age is a function of ambient conditions airplane and wind characteristics
B-727	Rear 3	169,000	108	1650	7.67	159	152	3309	5.3[c]	200[x]	4.9	
B-747	Wings 2	710,000	195.6	5500	6.95	195	163	7700	20.0[s]	122[c]	6.6[(1)]	
DC-9	Rear 2	108,000	89.3	934	7.40	165	154	2500	4.0[c]	200[x]	4.5	
DC-10	Wings 1 and Rear 1	410,000	155	3550	6.8			5595	9.4[c]	190[x]	5.8	
L-C5A	Wings 2	764,000	222.7	6200	7.20	161	150	7260	20.0[c]	115[x]	5.1	
L-1011	Wings 1 and Rear 1	409,000	155	3755	6.4			5581	7.9[c]	225[x]	5.7	

x = experimentally recorded maximum tangential velocity in tower fly-by at NAFEC

c = calculated parameter

s = estimated parameter

where

$\frac{dz}{dt}$ = vortex rate of descent

V_o = aircraft landing speed

C_L = operating lift coefficient, 1.34 for the B-707 and 1.49 for the B-747

A = wing aspect ratio

On all other aircraft the vortex rate of descent has been calculated by:

$$\frac{dz}{dt} = \frac{\Gamma}{2\pi b} \tag{2-3}$$

where:

$\frac{dz}{dt}$ = vortex rate of descent

Γ = circulation

b = wing span

Information on the core velocity is limited. In general, core models yield monotonically increasing tangential velocities as the radial distance increases. A transition to the line vortex equation (2-1) is made at this boundary. The tangential velocity beyond the core may then be calculated by this or more sophisticated models[2,3,4]. The values in Table 2-I are thus good approximations, which support the statement that maximum tangential velocities of the order of 100 ft/sec to 200 ft/sec at vortex descent rates of about 6 ft/sec are representative of the class of aircraft of interest to our study. Vortex core axial velocities are small and theoretically yet unresolved. They are assumed to be about 10% of the aircraft speed. Thus, in a landing configuration, an axial core velocity of 20 ft/sec may be representative.

The characteristic time τ for the onset of vortex instability is given by:

$$\tau = \frac{2\pi b^2}{\Gamma} \qquad (2\text{-}4)$$

where:

τ = vortex break up time

b = distance between vortices

Γ = circulation

For the two vortices trailing from the wing tips of contemporary airplanes, the characteristic time of instability is of the order of 3τ or one minute. If current information concerning the speeds at which various instability mechanisms propagate is examined, it can be concluded that[5] these speeds are much smaller than the velocity of trailing aircraft holding a flight pattern over an airport. Hence, any trailing aircraft will be interacting with the flow field of an undisturbed vortex.

2.3 JET ENGINE EMISSIONS

The use of jet engine exhaust and thermal emissions as indicators of the presence of vortex trails is dependent on the diffusion rates and mixing characteristics of these into the contrail structure. Such emissions will diffuse out into the jet regime, a distance of about 2 km, in a time frame of about 10 seconds, and then for another 2 minutes these exhaust products will become immersed in the developing vortex field that extends a distance of about 20 km. Finally, after the vortex break-up occurs the exhaust will be dispersed by the ambient atmosphere as a result of wind shear, residual wake turbulence and gravitational collapse. This total dispersion lasts for about 15 minutes after the vortex has been broken up. The detailed transport processes and chemistry that will determine the reaction rates, diffusion coefficients and thermal gradients in the vortex, are

presently not known. Hence, information on the concentrations of these pollutants in time and space along the vortex contrails, their decay rates or chemical transformation properties cannot be determined. Yet, such information is essential to assess the applicability of active radar, optical and spectroscopic techniques or passive radiometric measurements to the identification of the presence of the wake. The need for establishing these wake properties becomes essential and studies along these directions should be initiated. We shall, at the present, content ourselves with a classification of such jet engine emissions.

The constituents in jet engine exhaust under typical take-off or cruise conditions are tabulated in Table 2-II.[6]

CONSTITUENTS	SOURCE	ESTIMATED CONCENTRATION
N_2	Air	77% (Vol)
O_2	Air	16.6% (Vol)
A	Air	0.9% (Vol)
H_2O	Eff. Combustion	2.7% (Vol)
CO_2	Eff. Combustion	2.8% (Vol)
CO	Ineff. Combustion	10-50 PPM
Unburned HC	Ineff. Combustion	5-25 PPMC
Partially Oxidized HC	Ineff. Combustion	
H_2	Ineff. Combustion	5-50 PPM
Smoke (Particulates)	Ineff. Combustion	0.4-50 PPM (Mass)
NO, NO_2	Heating of Air	50-400 PPM
SO_2, SO_3	Fuel	1-10 PPM
Trace Metals	Fuel	5-20 PPB

Table 2-II. Engine Exhaust Constituents. Fuel is commercial Jet A-1 kerosene.

The constituents have been grouped by source into five different categories. These include 1) inert substances and unreacted oxygen from air, 2) products of complete combustion of fuel, 3) products of incomplete combustion, 4) oxides of nitrogen formed during the heating of air, and 5) elements or compounds derived from sulfur and trace metals present in kerosene fuel. The products of incomplete combustion include carbon monoxide; unburned fuel; partially oxidized hydrocarbons; hydrogen; and particulates (soot), consisting mainly of carbon.

Oxides of nitrogen are formed from the reactions of oxygen and nitrogen at the elevated temperatures in the reaction zone of the combustor. These oxides of nitrogen (NO_x) generally consist of 90 to 95 percent nitric oxide (NO) and the remainder nitrogen dioxide (NO_2). The quantity of nitric oxide formed is affected by a number of factors, including engine compressor pressure ratio, flight Mach number, fuel air ratio, and combustor design.

Commercial specifications for Jet A-1 kerosene require that the sulfur concentration in the fuel not exceed a value of 0.3 percent by weight. In practice, the sulfer concentration is generally less than 25 percent of this value. The sulfur in the fuel is mostly converted into sulfur dioxide (SO_2), with lesser amounts of sulfur trioxide (SO_3). A variety of trace metals are present in the fuel, such as aluminum, iron, manganese, nickel, sodium, potassium, and vanadium. The total concentration of the trace metals in jet engine exhaust is estimated to be about 5--20 parts per billion.

The presence of H_2O, NO_2, Hydrocarbons and smoke particulates in the vortex trail of the aircraft provides us with possibilities of detecting their presence by active or passive remote sensing techniques and therefore inferring the presence of the vortex trail.

REFERENCES - SECTION 2

(1) Hoshizaki, H. et al: "Study of High Altitude Aircraft Wake Dynamics", Report No. DOT-TST-73-5, January 1973.

(2) Hoffman, E. R., and Joubert, P. N., "Turbulent Line Vortices", Journal of Fluid Mechanics, Vol. 16, Part 3, pp 395-411, July 1963.

(3) Govindaraju, S. P., and Saffman, P. G., "On the Flow in a Turbulent Trailing Vortex", California Institute of Technology, AFOSR-69-1804.

(4) Squire, H. B., "The Growth of a Vortex in Turbulent Flow", 16,666, Aeronautical Research Council, 1954.

(5) Madden, S. J. and Harlan, R. B.,: "A Program to Analyze and Model Trailing Vortices on Airports", Final Report RN-69, Measurement Systems Lab., Department of Aeronautics and Astro-Nautics, M.I.T., Cambridge, Mass., October 6, 1971.

(6) Grobman, Jack: "Jet Engine Emissions", pp25-33, NASA TMX 68221, Measurement of High Altitude Air Quality Using Aircraft, AIEEC Conference, Denver, Colorado, June 1972.

SECTION 3

STUDY OF IN-FLIGHT MEASUREMENT TECHNIQUES AND INSTRUMENTATION SYSTEMS

The determination, by its own independent means, of the presence of a vortex pair shed by an aircraft in the vicinity of the landing corridor may be helpful to the approaching aircraft in the line of flight of the first. This measurement may help the second aircraft avoid the effect of the vortices shed by the first, in a sufficient time. During the landing phase, the aircraft may thus generate its own information with respect to the presence of other vortices in its flight path. This information, available at a most crucial time in the landing approach zone of the aircraft, will supplement any other vortex location information generated further down the glide path by the ground based Aircraft Trailing Vortex Warning System (ATVWS). Similarly, at departure, any information available to the aircraft, at a critical range from the airport, but outside of the coverage provided by ATVWS, will help the pilot secure a smooth and safe ascent path.

A desirable feature of any such airborne vortex remote sensing instrumentation system is that it operates as an extension of or in conjunction with presently on-board flight instrumentation. Weather radar, which is standard equipment on all commercial airliners, would ideally serve as a useful indicator of the presence of vortex trails in the vicinity of the flight path. The feasibility of using any one instrumentation technique is a function of the physical characteristics of a trailing vortex and how well it lends itself to remote detection. A signature left behind by the vortex, a) due to its motion, b) as a result of the secondary effects generated by its velocity

field on the surrounding atmosphere, or c) due to the physical mechanisms inherent in the jet engine emission products entrapped by the vortex, generates physical observables by which the presence of the trails may be identified. The physical characteristics of trailing vortices that generate various signatures in the atmospheric environment have been previously reviewed. We will now examine these characteristics in detail and analyze the feasibility of applying various instrumentation systems to the problem. Conceptually, a number of technical approaches based on active and passive remote sensors, which may be used to secure information about the vortex characteristics exist. These potential systems may exploit:

a) the scattering of microwaves from index of refraction variations in the atmosphere generated by the vortex turbulence.

b) the Doppler shift induced at 10.6 microns in pulsed or CW CO_2 laser radar due to scattering with particles entrained in the vortex.

c) the scattering of acoustic waves from index of refraction change and Doppler shift variations in the vortex trail.

d) the heat content in the vortex and its detection by infrared radiometry techniques.

e) water vapor and nitric oxide jet engines pollutant absorption and emission spectra in the far infrared.

We will now explore the system configurations related to these techniques and their practical applicability to the vortex detection problem. Our aim, in this study, is to arrive at possible system configurations that from a practical point of view are the simplest and most cost effective to realize. The ultimate realization of any such measurement system may depend on undertaking an experimental

measurements program and further developing the theoretical understanding necessary for the application of the techniques.

3.1 APPLICATION OF ON-BOARD WEATHER RADAR SYSTEMS TO VORTEX DETECTION

Radar weather systems presently on-board aircraft are primarily used for weather and terrain mapping. The technical feasibility of using this instrumentation for the in-flight detection of vortices is an attractive possibility. Such a system in conjunction with ground-based vortex detection instrumentation systems or on a stand-alone basis may enhance the arrival and departure safety criteria of aircraft operating in crowded airport terminals without the need for additional equipment. What must be ascertained, then, is to determine whether:

a) the present on-board radar instrumentation can be used for this additional task

b) modifications, if any, may, at a minimum cost, convert the present weather radar systems to perform this task

c) the sensitivities and operational characteristics of these systems limit the ultimate performance expected from an on-board in-flight vortex detection system and

d) it may be most advantageous to develop a new concept requiring additional on-board equipment, specifically designed to measure in-flight vortices.

A typical system presently used on-board commercial airlines is the Bendix RDR-IE/ED Weather Radar System. This system provides the pilot with a visual indication of storm conditions at ranges up to 300 miles. This visual indication permits the pilot to distinguish corridors of relatively calm air through the storms, thereby enabling him to avoid areas of high turbulence without making

long costly detours. In addition to its principal function of weather mapping, the system also provides valuable terrain mapping data[1]. The characteristics of this system are as follows:

Frequency:	9375 ± 40 MHz
Wavelength:	3.2 cm
Band:	X-Band
Range:	Maximum range of 300 nautical miles with 30" antenna
Transmitter Power Output:	50 KW - 75 KW
Pulse Width:	2.5 and 5.0 microseconds
PRF:	400 ± 20 Hz
System Noise Figure:	7 dB
Antenna Scan Angle:	120^{o}, 180^{o} or 240^{o}
Antenna Beam Width:	3^{o} for 30" reflector

Figure 3-1 illustrates the location of the radar on-board an aircraft and depicts the limits of beam coverage in range, elevation and azimuth. A new digital display weather radar system has been recently introduced by Bendix[2]. This RDR-1200 Weathervision System incorporates a digital display indicator that allows the pilot to observe total target information at any time, regardless of the position of the antenna. The system includes a 10 KW X-band receiver/transmitter incorporating a coaxial magnetron, with a 12" flat-plate phased-array type antenna, providing a range of 200 nautical miles. Applications for this system are primarily aimed at business aircraft, commuter airlines, and non-tactical military aircraft. First units of this system are now available and sell for about $18,000.

It is the purpose of this study to determine whether or not such a system or its equivalent does show promise, after required modifications, to indicate the presence of trailing vortices. Let us

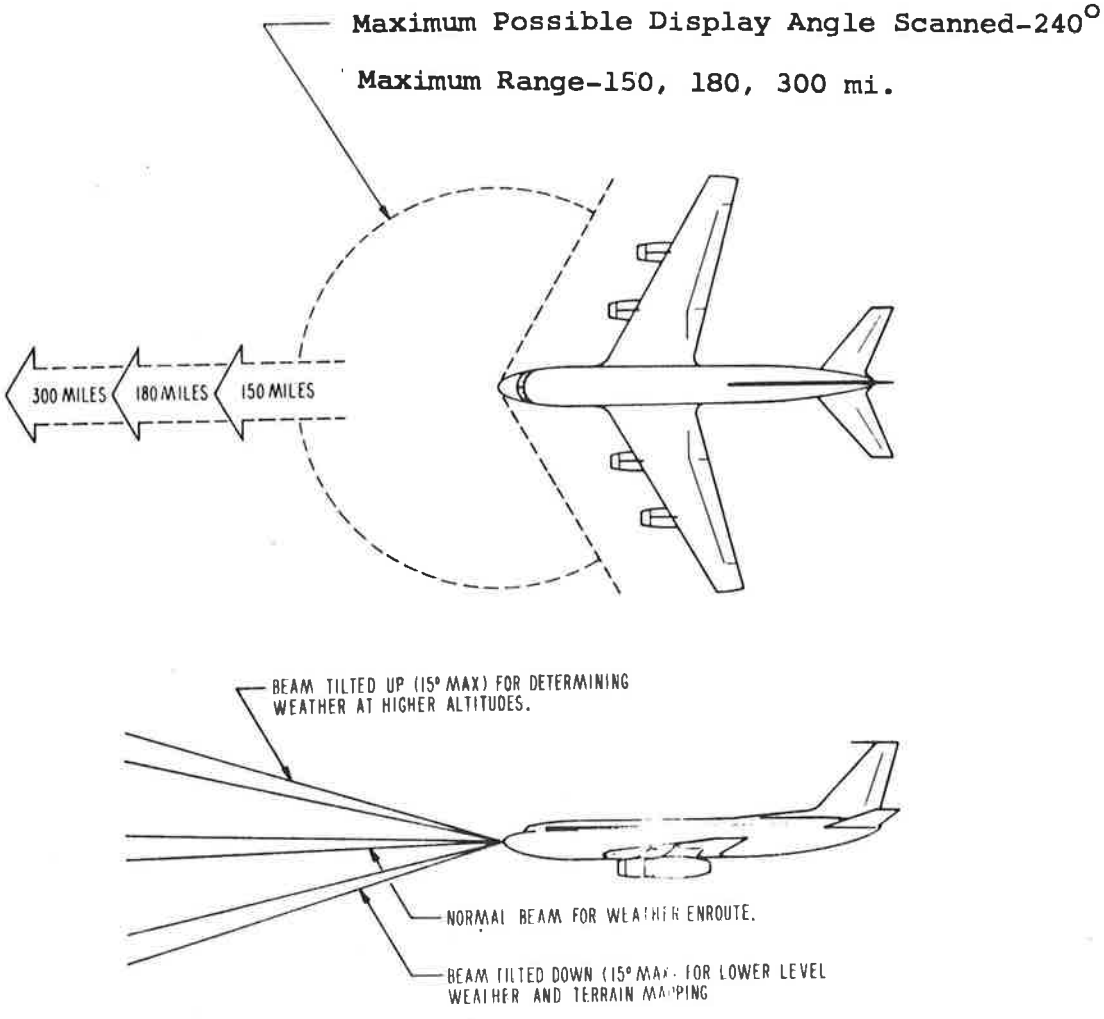

Figure 3-1. RDR-1E Airborne Weather Radar System

then review the physical mechanisms that are prerequisite to obtain meaningful electromagnetic energy returns from a vortex.

3.1.1 DETECTION OF VORTEX TURBULENCE BY ELECTRO-MAGNETIC RADAR TECHNIQUES

An active microwave radar probe of a trailing vortex can detect its presence by a measurement of a) the Doppler scatter from particulate matter or b) the volume scatter from regions of index of refraction discontinuieties. Such systems require that the signal received from the target must be of a sufficient intensity at the required signal-to-noise ratios to be compatible with detectors, pre-amplifiers or other elements of the receiver electronics.

3.1.1.1 Microwave Doppler Radar

Particulate matter found in the atmosphere, primarily aerosols, range in radius from 0.001 to 100 microns[3]. Such liquid and solid particles follow the motion of air, on the average, and can be used as indicators of air motion and turbulence. In the measurement of aircraft wake vortices, during take-off or landing, particulate products of the jet emissions such as soot will diffuse into the wake, increasing the concentration of aerosol particles already entrapped therein. At X-band, however, a wavelength of 3.2 cm is not an optimum match to the size of the particulate distribution in the wake. Calculations show that the scattering cross-section will be extremely small, possibly of the order of 10^{-21} m^2 for a particle size distribution larger than 3 microns and 10^{-32} m^2 for a particle size distribution of the order of 0.1 microns.[3] It is only at laser wavelengths, in the visible or the infrared, that the size of particulate matter becomes comparable to a wavelength, resulting in Mie-scattering. This, as will be

shown in Section 3.2, results in a level of scattered power and signal-to-noise ratios that are compatible at the output of a detector for vortex detection and display purposes.

Microwave Doppler measurements may best be performed by scattering from chaff seeded into the wake or by obtaining returns, during approach to an airport, under snow conditions. Such work has been performed[5] and is, for obvious reasons, not suitable for our purpose. Thus, it may be concluded that scattering from atmospheric aerosols present in the wake at microwave frequencies is negligible.

3.1.1.2 Radar Reflections from Regions of Atmospheric Refractivity Inhomogeneities Generated by Wake Vortices

Scattering from fluctuations in the refractive index of the atmosphere has provided a very powerful tool in the application of high power, steerable radars to clear air turbulence (CAT) investigations. It has been clearly established[6,7] that sensitive radars with megawatts of peak power and wavelengths of 3.2 cm can detect echoes over a distance of 10 KM caused by backscattering from inhomogeneities of refractive index in the atmosphere. There are two ways by which radar backscattering provides information on atmospheric structure. First, the backscattered power is related to the intensity of fluctuations in refractive index within a narrow range of turbulent eddy sizes, centered at one half the radar wavelength. Second, through an analysis of the echo regions and patterns outlined by the radar, the gross discontinuities in the atmosphere due to the presence of turbulence can be delineated. Water vapor is the primary contributor to refractive index variations in the atmosphere, while positive buoyancy forces significantly contribute to the generation of small scale turbulence.

The theory of the scattering of electromagnetic waves from refractive index fluctuations has been treated by Tatarski[8]. Its application to CAT measurements in the atmosphere has been worked out by Ottersten[9] who has derived expressions relating radar reflectivity to the intensity of refractive index variations. References (6) and (7) are excellent summaries of this work. The purpose of this investigation is to ascertain whether a similar concept of radar measurements, limited to reasonable modifications of presently on-board weather radars can be applied to the measurement of the wake vortex induced turbulence.

In the turbulence associated with aircraft trailing vortices, entrainment of the heated engine exhaust and diffusion of the water vapor content of the jet engine emission may result in a variation in the refractive index along the contrails. When air parcels are displaced in the atmosphere by mixing, inhomogeneities are created because the characteristics of the displaced air parcels will differ from those of the environment. The pressure of the displaced parcels undergoes a continuous equalization with the environmental pressure. This process will change the temperature and water vapor pressure of the air parcels. Their potential temperature and specific humidity, however, will be preserved. The displaced air parcels in the vortex will, to the first approximation, keep their identity. Consequently, the resulting inhomogeneities in refractive index within the vortex are best characterized by the differences in potential temperature and specific humidity or of potential refractive index between the regions exchanging air parcels. The sharper the original mean gradient and the more violent the turbulent mixing the stronger will be the inhomogeneities which are created, and consequently the radar scattering will be increased. Similarly, for a given mean gradient of potential refractive index; the stronger the turbulence, the stronger will be the inhomogeneities.

The basic expression which relates the radar reflectivity, σ, or radar cross-section per unit volume, to the random refractive index fluctuations, for energy backscattered to the radar, is:

$$\sigma(\vec{k}) = 8\pi^2 k^4 \Phi_n(\vec{k}) \tag{3-1}$$

The direction of the vector wave number k is the radar's radial direction and it has magnitude $k = |\vec{k}| = 4\pi/\lambda$, λ is the radar wavelength, and $\Phi_n(\vec{k})$ is the spatial power-spectral density which is a three-dimensional representation of the refractive index field. $\Phi_n(\vec{k})$ is the Fourier transform of the three-dimensional refractive index covariance function and is related to the variance of the refractive index $\overline{n'^2}$ by:

$$\int_{-\infty}^{\infty} \Phi_n(\vec{k})\, dk = \overline{n'^2} \tag{3-2}$$

where the integration is carried out over the entire wave number space. Although $\Phi_n(\vec{k})$ is defined for all wave number space, only one particular value of the wave number contributes to the radar backscattering. The radar essentially samples the refractive index spectrum at the particular wave number vector which is directed along the radar radial direction and has a magnitude of $4\pi/\lambda$. This wave number corresponds to the spatial scale of $L = 2\pi/k = \lambda/2$. The eddy sizes near $\lambda/2$ contribute to the backscatter because it is only these sizes that produce additive phases and that consequently produce a signal which is detectable at the receiver. The only requirement is that some spectral energy is present at a scale of $\lambda/2$. The process is identical to constructive interference of the waves diffracted by the appropriate spacing of the grating for Bragg scattering.

The turbulence characteristics of the vortex are generated primarily by a discontinuity in the air flow, traversing the wings, causing a vortex flow to be shed along the wing tips. The velocity gradients thus generated across the width of the vortex core in combination with fluctuations due to a) heat emissions from the engines, b) humidity content of the exhaust and c) ambient atmospheric effects, will form the bulk of the resultant turbulence along the contrails of the airplane. The net effect of all these contributions leads to fluctuations in the density; hence, the refractive index structure of that portion of the atmosphere along which the vortex trail propagates. The variance of the refractive index, (see Equation 3-2), is defined by the structure function of refractivity. Following Tatarski, one can then define a structure parameter of the refractivity, C_n, pertaining to the vortex trail, i.e.,

$$D_n(r) = \langle |n(x) - n(x + r)|^2 \rangle_{AV} = C_n^2 r^{2/3} \qquad (3\text{-}3)$$

where:

$D_n(r)$ = structure function of refractivity
C_n = structure parameter of refractivity
r = spacing between two points

If one assumes within the vortex trail isotropic turbulence, a condition yet unsupported by experiment, then the radar cross-section can be related to C_n. As such,

$$\sigma(\vec{k}) = 0.38\, C_n^2\, \lambda^{-1/3} \qquad (3\text{-}4)$$

Since the radar cross-section per unit volume is proportional to $\lambda^{-1/3}$, larger cross-sections can be measured for a given index of

refraction structure change in the trail, at smaller wavelengths. However, a seven-fold decrease in the wavelength, from a microwave frequency of 10 GHz up to a millimetric wave frequency of 70 GHz, will only increase the radar cross-section by a factor of 2.

There does not exist, at the present time, experimental work on vortex turbulence that defines the structure function parameter and yields a measure of the radar cross-section as a function of wavelength. Work presently in progress at NASA Laboratories[10] and using laser Doppler techniques, addresses itself to the measurement of the power spectra density of the vortex turbulence in simulated flow environments. The results of this work may eventually lead to the quantities stipulated above. A model, sufficiently accurate for our purposes, however, has been derived,[3] in which only the contributions of temperature fluctuations in the wake are taken into account. This model yields a formula for the backscattering cross-section, independent of wavelength for a vortex at an average temperature ΔT above ambient, i.e.,

$$\sigma_B \sim \frac{1}{2\pi} \frac{P_o^2}{T_o^4} \overline{(\Delta T)}^2 \frac{V}{L_T} \times 10^{-8} \qquad (3\text{-}5)$$

where:

σ_B = scattering cross-section, sq. metres
P_o = atmospheric pressure, millibars
T_o = atmospheric temperature, ^oK
V = volume of vortex wake, m^3
L_T = correlation length for temperature, m

Taking $\overline{(\Delta T)}^2 \frac{V}{L_T}$ to be of unity order, with $P_o = 10^3$ millibars and $T_o = 300^oK$, one finds $\sigma_B \sim 2 \times 10^{-13}$ sq. metres. If the temperature differential in the wake is 10^oK and the correlation length is 1 cm (corresponding to a wavelength of 2 cm) over volumes of a cubic metre, the

cross-section can be of the order of 10^{-9} sq. metres. Thus, we will assume in the absence of any available experimental evidence, that radar backscattering cross-sections will vary between 10^{-13} and 10^{-9} sq. metres.

3.1.1.2.1 Radar Detection of the Vortex Trail

The radar equation yields the maximum range over which a target of cross-section σ, may be detected as a function of the radar transmitter and receiver parameters. Thus,

$$R_{Max} = \left(\frac{P_T \rho A_R^2 \sigma \sqrt{n} e^{-2\alpha R_{Max}}}{4\pi \lambda^2 S_{Min}} \right)^{1/4} \qquad (3\text{-}6)$$

where: R_{Max} = Maximum detectable range, metres
P_T = Peak power per pulse, watts
A_R = Receiving antenna aperture, sq. metres
σ = Target cross-section, sq. metres
λ = Radar wavelength, metres
S_{Min} = Minimum detectable signal, watts
n = Effective number of pulses integrated
α = Attenuation constant of propagation medium, metres^{-1}
ρ = Antenna efficiency

and the radar pulses are integrated non-coherently, since the phase of the return signal is not preserved.

We want to investigate the feasibility of applying the presently used 10 GHz, X-band weather radar, whose characteristics have been summarized in Section 3.1, to the problem of detecting the vortex trail defined by radar cross-sections in the 10^{-13} to 10^{-9} sq. metre range. Further, we also will determine the feasibility of detecting the vortex at millimetric wavelengths, at frequencies of 35 GHz and 70 GHz. The application of recent pre-amplifier and transmitter technology developments in the 10 GHz to 70 GHz frequency range

is imperative. Figure 3-2 shows the presently available noise performance characteristics of microwave and millimetric wave receivers.[11]

Table 3-I summarizes the minimum detectable signal levels and transmitter peak powers that can be presently attained.

TABLE 3-I. State-of-the-art Microwave and Millimetric Wave Transmitter-Receiver Characteristics

Frequency GHz	PRF	Transmitter Type	Transmitter Peak Power	Max. Pulse Duration (μs)	S_{Min}/MHz Bandwidth	Receiver Front-End
9.373	1000	Pulsed Magnetron	75kW	1.0	7×10^{-15} watts	Non-degenerate room temperature parametric amplifier
	500	Pulsed Magnetron	1000kW	2.0		
35	1000	Pulsed Magnetron	150kW	0.6	5.4×10^{-5} watts	Cryogenic non-degenerate parametric amplifier
					4.22×10^{-5} watts	Traveling wave Maser
70	3300	Pulsed Magnetron	10kW	0.3	4.75×10^{-5} watts	Traveling wave Maser

The following are the system parameters:

Antenna Diameter:	60 inches
Attenuation Characteristics[12]	0.003 dB/km at 10 GHz
	0.025 dB/km at 35 GHz
	10 dB/km at 70 GHz
Antenna-Receiver Efficiency:	0.8
Pulse Integration Time:	1 second post-detection integration

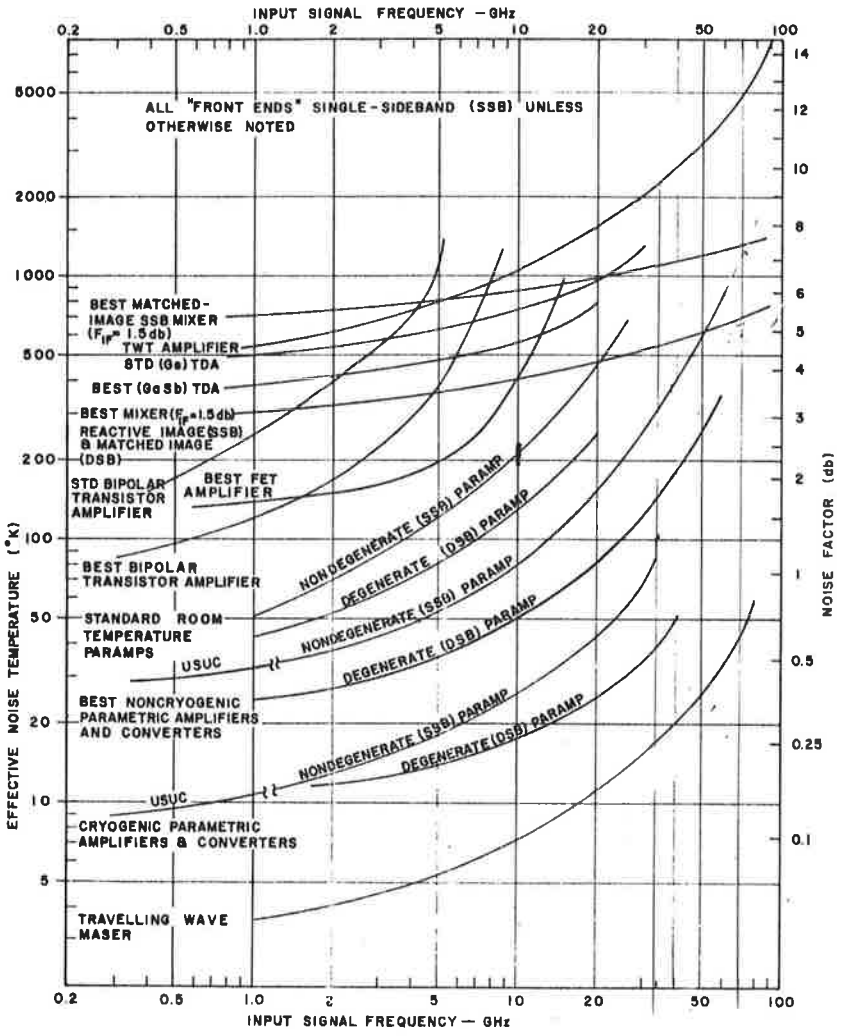

Figure 3-2. Receiver Front-end Noise Performance as Function of Input Signal Frequency -- State-of-the-art.

Receiver Noise Figure:	As per Table 3-I.
Radar Cross-section:	10^{-13} to 10^{-9} sq. metres

Equation 3-6 has been evaluated for the above system parameters and the resultant R_{Max} vs. σ relationships are shown in Figure 3-3.

The present weather radar system, in conjunction with a 2.4 dB noise figure parametric amplifier, can attain a maximum range of 1.6 km under the best of assumed wake vortex radar cross-sections. If the system is modified to a 100 KW per pulse transmitter, with a 60" diameter dish and a 2.4 dB noise figure parametric amplifier a maximum range of 4.5 km is attainable. At 35 GHz, with a transmitter of 150 KW and 0.25 dB noise figure Traveling Wave Maser a maximum range, within the desired range of 6.5 km, is attainable. A transmitter at 70 GHz is totally ruled out because severe atmospheric attenuation due to absorption by atmospheric oxygen completely limits system performance. It is necessary to perform experimental measurements on such a radar system to assess the actual radar cross-section generated by the vortex. However, such a modified system may prove feasible.

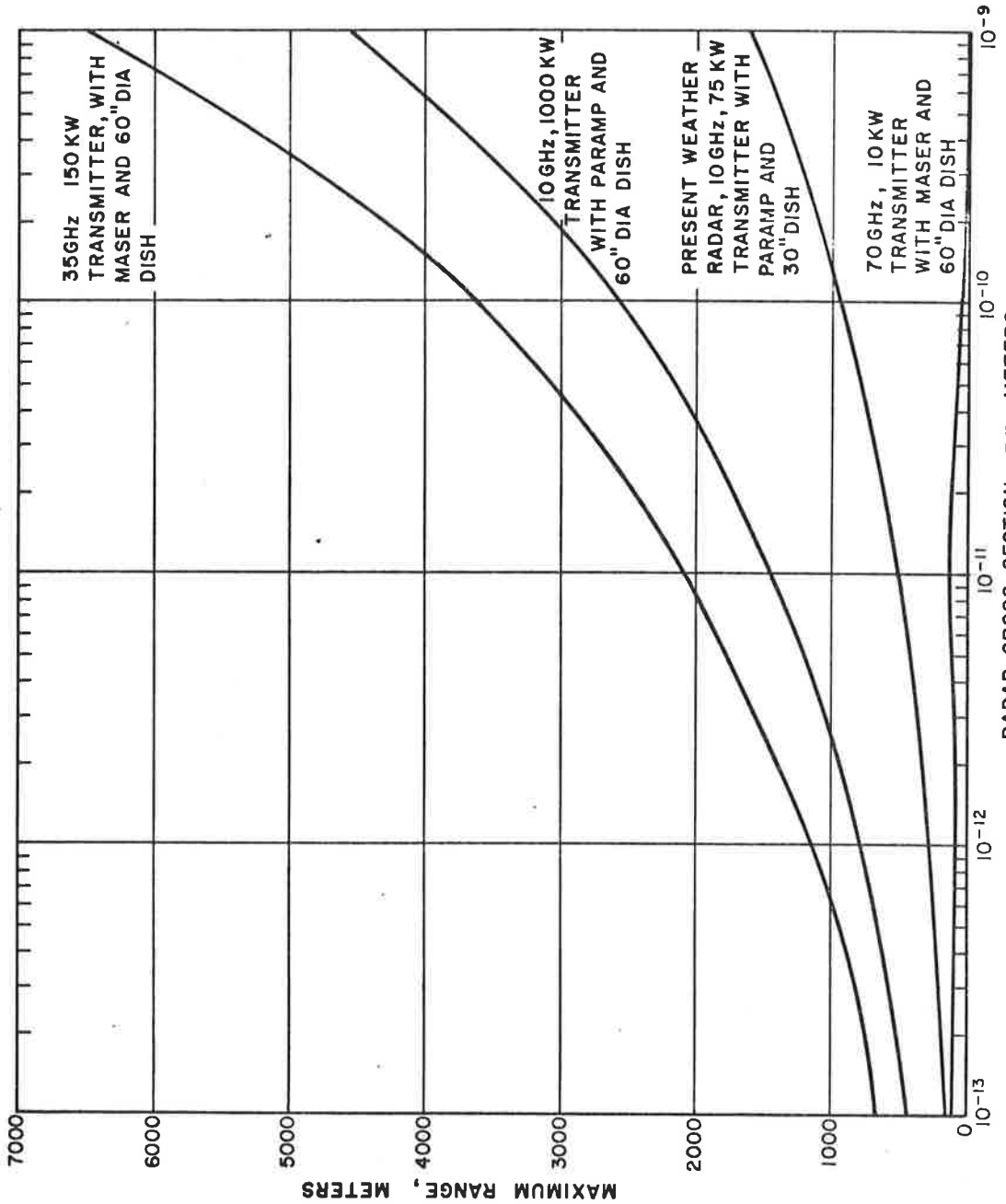

Figure 3-3. Estimated Maximum Vortex Detection Range Attained with Modified Weather Radar.

3.2 APPLICATION OF OPTICAL RADAR TO VORTEX DETECTION

Lasers have been applied in numerous remote sensing applications as optical radars in order to measure atmospheric conditions, to identify pollutants, and to define the properties of atmospheric aerosol scatterers. These systems have presently reached an impressive stage of technological maturity where they can be applied from ground stations and in-flight platforms to perform quantitative remote measurements of atmospheric characteristics. Laser devices for cloud observations and visibility measurements are in development[13]. Meteorological laser systems capable of measuring vertical profiles of water vapor, temperature, aerosol concentrations, identify gaseous pollutants[14], measure wind[15] and clear air turbulence conditions[16] have been used and their feasibility demonstrated. Laser radars have been used to measure aircraft trailing vortices and results obtained have been successfully correlated with visual observations[17]. In laboratory, under transonic wind tunnel flow conditions, such vortices have been analyzed by laser Doppler techniques and the results satisfactorily compared against hot wire anemometers[18,19].

Atmospheric information obtained by laser probes depend on the interaction of the transmitted laser energy with the atmosphere. Atmospheric interactions, taken on a macroscopic scale, attenuate the transmitted energy and introduce fluctuation of amplitude and phase. This extinction of the transmitted energy is the result of its

attenuation due to absorption by the species of the atmosphere and scattering by particulate interaction and atomic processes. It is, in principle, this scattered light that yields the information concerning the atmosphere.

We shall be concerned with the application of lasers in the visible and infrared bands to determine whether either by Light Detection and Ranging (LIDAR), coherent detection or spectroscopic identification of the wake particulate and emission products, it is possible to detect the presence of a trailing vortex.

3.2.1 LIDAR MEASUREMENTS ON TRAILING VORTICES

Light Detection and Ranging Measurements in a trailing vortex may be performed by detecting an amount of back-scattered energy collected at an optical receiver aperture as a result of illuminating the vortex with a laser beam. In Table 3-II, the prominent characteristics of presently available Ruby, Nd:YAG and CO_2 lasers that may be used in the detection of vortices from in-flight platforms are tabulated.

TABLE 3-II. Laser Characteristics

	Ruby	Nd:YAG	CO_2	CO_2 Q-switched
Wavelength, λ	0.6943	1.06	10.6	10.6
Pulse Width, τ	10-20 nsec	20 nsec	cw, 2 μ sec-10 μ sec	0.2 μsec
PRF, sec^{-1}	1,1/3	50	200	30,000
Energy/Pulse	1.5j, 7.5j	100 mJ	20 mJ	0.1 mJ
Peak Power	150MW, 750MW	5MW	10KW, 2KW	500 W
Average Power	1.5W, 2.5W	5W	4W	3 W

Ruby and Nd:YAG are pulsed solid state lasers that generate a multimode incoherent beam whereas the CW CO_2 laser with a single frequency and single mode may be modulated to generate a coherent train of pulsed radiation. Thus, while Ruby and Nd:YAG lasers are candidates for a Lidar, the pulse-modulated CO_2 laser can be used for performing optical Doppler measurements in the trailing vortex.

The basic lidar equation for the calculation of signal returns will now be derived. Using the geometry of Figure 3-4, we assume a pulsed transmitter of pulse width τ, and peak power P_T, and calculate for an observed range gated atmospheric cell the number of signal photoelectrons returned to the monostatic receiver.

The basic assumption in this calculation is that returns from the vortex will be obtained from naturally occurring aerosols entrained in the flow field of the vortex, enhanced by carbon particulates which are emitted from the jet engines. Information about this soot as to its particulate size, concentration and extinction coefficient is scant. Thus, its presence in the wake may increase the amount of backscattered energy beyond the level to be calculated by the assumption made.

The number of signal photoelectrons derived at the terminals of a photo multiplier as a result of backscattering from aerosols contained in the sampled resolution cell of the Lidar is:

$$P_S = E \times e^{-\mu R} \times \frac{c\tau}{2} \times \beta(\pi) \times \frac{A_r}{R^2} \times e^{-\mu R} \times \frac{\eta_{sy}\ \eta_D}{h\nu} \times G \qquad (3\text{-}7)$$

= energy/pulse x attenuation to target over range x minimum size of range gate x backscattering coefficient at laser wavelength solid angular aperture of backscattered beam x attenuation to receiver over range x system efficiency x detector efficiency/energy per photon x Gain.

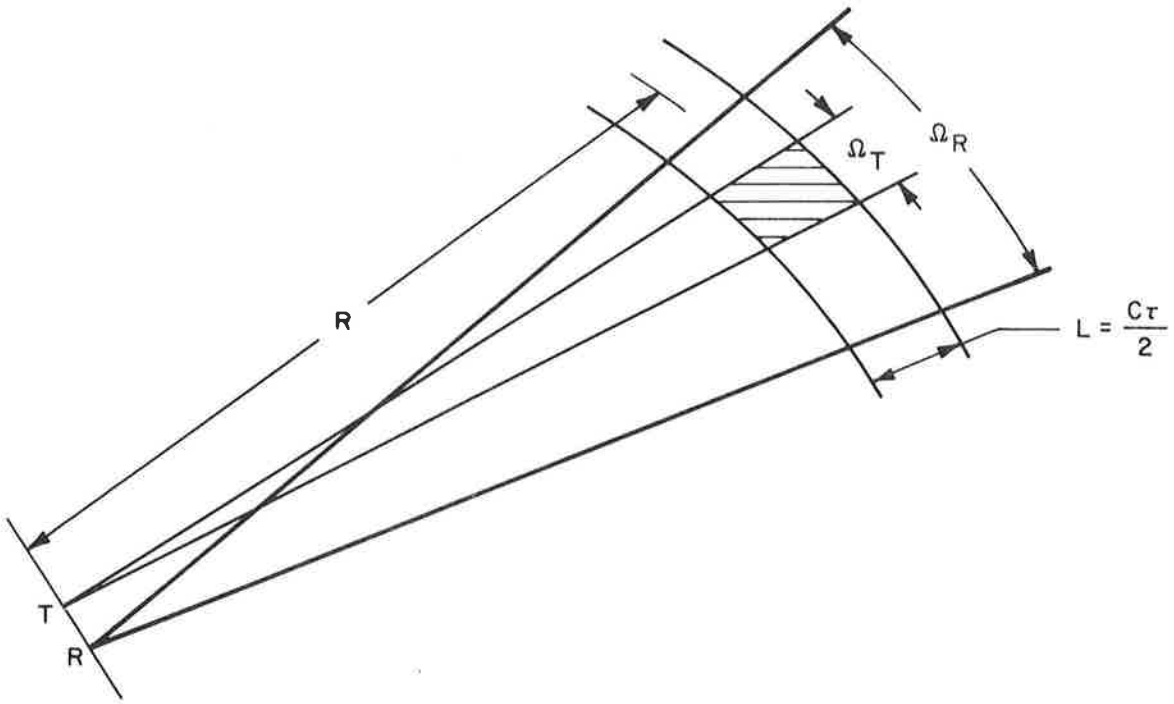

Figure 3-4. Lidar Configuration

i.e.,

$$P_S = \frac{E\, c\tau\, \beta(\pi)\, A_r\, e^{-2\mu R}\, \eta_D\, \eta_{sy}\, G}{2h\nu R^2} \qquad (3\text{-}8)$$

Symbol	Description	Value
P_S	Signal Photoelectrons	
E	Energy/Pulse	1.5 joules for Ruby 100 mjoules for YAG
τ	Pulse Width	20×10^{-9} seconds
μ	Attenuation Coefficient	
	clear air	0.15 km^{-1}
	light haze	0.3 "
	haze	0.1 "
R	Range	km
C	Speed of Light	3×10^{8} met/sec
$\beta(\pi)$	Backscattering Coefficient	
	clear air	5×10^{-6} m^{-1} sr^{-1}
	light haze	10^{-5} " "
	haze	2×10^{-5} " "
A_r	Receiving Optical Area	7×10^{-2} m^2 (12-inch transmitter)
η	Efficiency of Receiving Optics	0.50
η_D	Efficiency of S-20 Photomultiplier Detector	0.025
h	Planck's Constant	6.625×10^{-34} joule-sec
ν	Light Frequency or C/λ	4.34×10^{14} Hz
λ	Ruby Wavelength	0.6943×10^{-6} metres
G	Photomultiplier Gain	10^{6}

The noise photoelectrons are primarily contributed by the atmospheric background radiation, detector dark current and thermal noise. These noise sources are defined by:

Background noise: $$P_{n_{BG}} = H_{b\lambda} \times \Delta\lambda \times A_R \times \Omega_R \times \frac{\eta_{sy}\, \eta_D\, \tau}{h\nu} \times G \qquad (3\text{-}9)$$

Dark current noise: $$\bar{P}_{n_{DC}} = \sqrt{\frac{2I_D B}{q}}\, G\tau \qquad (3\text{-}10)$$

Thermal noise: $$\bar{P}_{n_J} = \sqrt{\frac{4kTBF}{R_{eq}}}\, \frac{\tau}{q} \qquad (3\text{-}11)$$

where:

Symbol	Description	Value
$\bar{P}_{n_{BG}}$	Average number of background photoelectrons/integration time	photoelectrons
$H_{b\lambda}$	Background radiation	10^{-3} watts m^{-2} sr^{-1} A^{-1} at 0.6943 μm
		2×10^{-4} watts m^{-2} sr^{-1} A^{-1} at 1.06
$\Delta\lambda$	Filter Width	20 Å
A_r	Receiver Area	7×10^{-2} m^2
Ω_R	Receiver FOV	3^o
η_{sy}	System Efficiency	0.50
η_D	Detector efficiency	.025
τ	Pulse width	20×10^{-9} sec
$\bar{P}_{n_{dc}}$	Dark current noise	photoelectrons
q	Electron charge	1.6×10^{-19} coul.
$\bar{P}_{n_J}$	Johnson noise of preamplifier	photoelectrons
K	Boltzmann's Constant	1.38×10^{-23} J/°K
R_{eq}	Resistance	50 ohms
T	Noise Temperature	300^o K
F	Preamplifier noise-figure	2 dB
I_D	Dark current	10^{-15} amps
G	Photomultiplier S-20 Gain	10^6

The signal-to-noise ratio that will result in the application of the ruby laser to detect the presence of the vortex trail by its

deployment as an incoherent energy detection Lidar is given by:

$$S/N = \frac{P_S^2}{\left(\sum P_{\overline{n}}\right)^2} \qquad (3\text{-}12)$$

The results of the computation SNR vs. Range for detection of back-scattered radiation are shown in Figure 3-5.

Evaluation of Equations 3-9, 3-10 and 3-11 shows that the background noise photoelectrons are of the order of 10^9, compared to 10^4 for the dark current noise and 10^3 for the thermal noise. At a range of 1 km, the 12" diameter transceiver with a 3 degree field-of-view will collect a total of 5×10^{10} signal photoelectrons, leading to a SNR, as shown in Figure 3-5, of about 23 dB. It has been shown that an incoherent detection Ruby Lidar system will not satisfactorily operate at ranges beyond 2 km. Since it does not, in addition, measure a characteristic signature of the vortex, the system is not useful in this application.

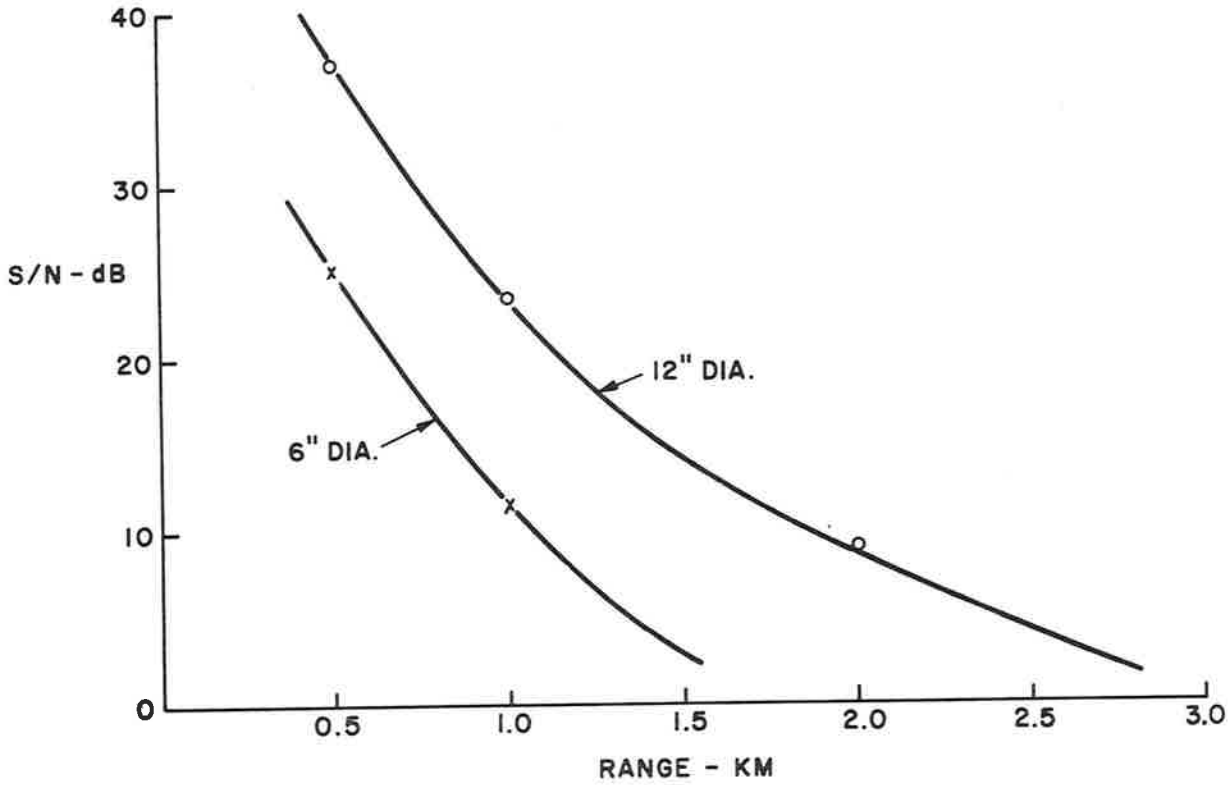

Figure 3-5. Incoherent Detection of Wake with Ruby Lidar, SNR vs. Range Relationship

3.2.2 DETECTION OF TRAILING VORTICES WITH CO_2 LASER OPTICAL DOPPLER RADAR

The returns received with a ruby lidar as a result of backscattering from atmospheric aerosols and jet engine particulate matter diffused into the wake may not constitute a fool-proof indication of the presence of the vortex trail. The lidar returns, in this incoherent energy detection scheme, do not measure a distinctive characteristic of the vortex trail. The received return when range gated with respect to the vortex location will, at best, indicate an increase in received signal level with respect to the quiescent atmosphere near and around the vortex limits.

In performing remote measurements on vortex trails, it is important to sense those of their intrinsic characteristics which will, without doubt, identify the vortex with respect to the atmospheric environment in which it is propagated. One such vortex characteristic which will identify it positively is its velocity distribution. The vorticity of the wake generates the much larger tangential velocity component of the vortex which lies in a plane orthogonal to the flight path of the aircraft. An aircraft following the first that sheds the vortex trails, must scan the space that its laser Doppler radar samples in order to acquire and track a component of the vortex velocity field that optimizes the Doppler returns obtained. Since the axial component of the vortex trail may be, at best, a factor of 10 smaller than the tangential velocity, a plane following another one may measure a distribution of Doppler shifts related to the velocity components in the line-of-sight of its scanning Doppler radar. In section 3.2.2.3, numerical estimates of the range of Doppler shifts that may be measured are given.

As the vortex is formed behind an airplane, the various dust particles, water droplets and other particulate impurities that make

up the atmospheric aerosol will be entrained in the vortex. These particles will be distributed within the vortex space over intra-particle distances many times larger than the illuminating laser wavelength, thus forming a diffuse target. If scatterers are densely distributed with separations much less than a wavelength, the scattered radiation tends to be fully coherent. When the separations between the particulate matter are many wavelengths in size, the random positions and velocities of the particles cause the scattered radiation from one particle to be incoherently related to that from any other particle when averaged over a small time interval.

In the application of microwave Doppler radar, the atmospheric and engine particulates entrapped in the vortex have intraparticle separations which are significantly shorter than a wavelength, with the result that the return that is obtained is completely coherent and not diffused. The laser radar, however, with its shorter wavelength illuminates a target where particles are on the average many wavelengths apart. Equations relating signal-to-noise ratios to the range when detecting such returns have been derived[20] and will be used to evaluate the feasibility of applying CO_2 laser Doppler radar to the detection of the velocity distribution in trailing vortices.

3.2.2.1 Laser Doppler Radar

Photomixing offers a means of realizing coherent optical detection. Figure 3-6 shows a typical coherent and incoherent receiver configuration. In coherent detection an important distinction arising with respect to non-coherent detection, previously discussed in Section 3.2.1, is the addition of a reference local oscillator signal prior to the detector. The local oscillator reference is then made to have an amplitude much larger than the input signal or noise, effectively operating the detector at its shot-noise limit.

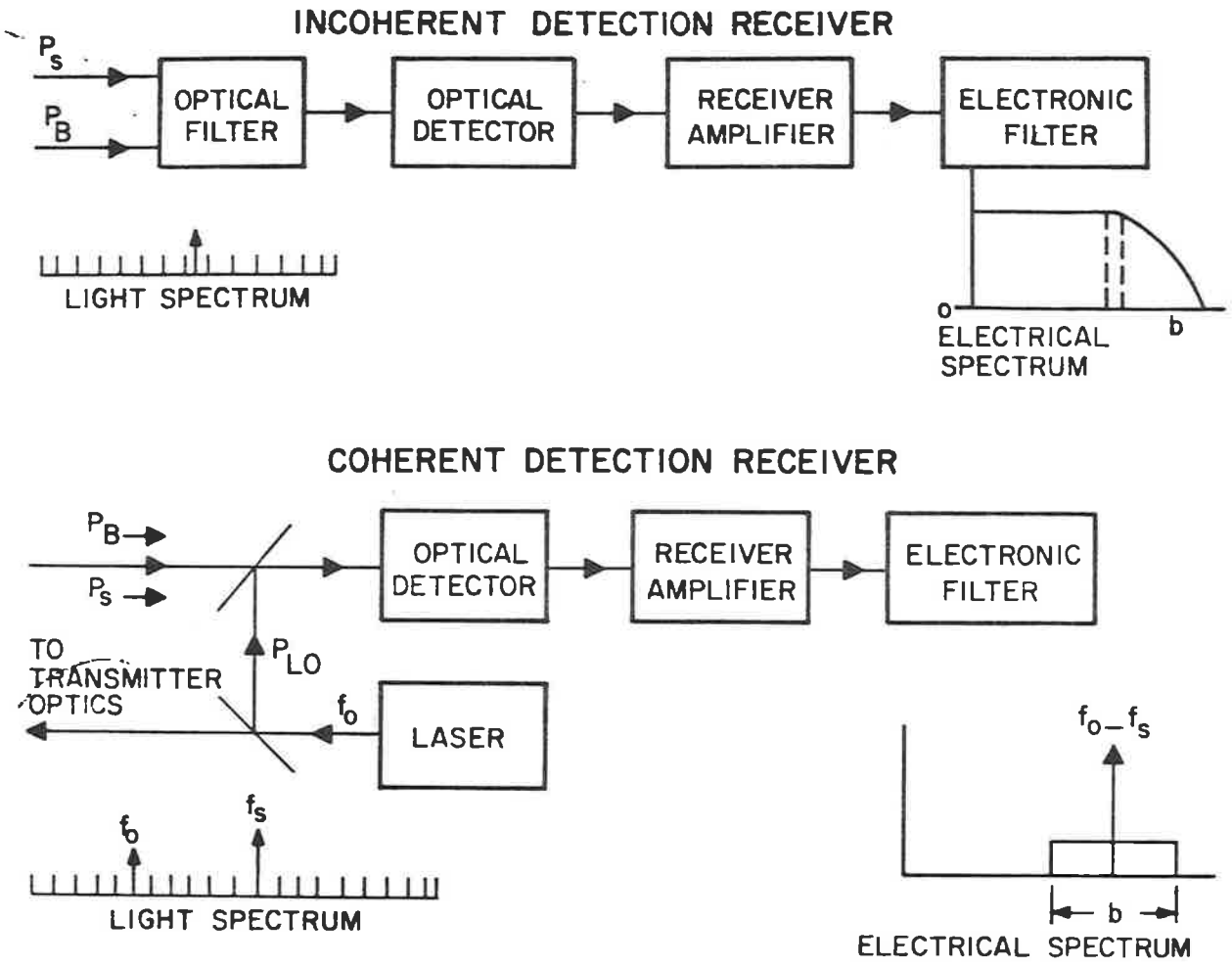

Figure 3-6. Receiver Configuration

The signal-to-noise ratio that will result at the output of the detector can be shown to be :

$$S/N = \frac{\eta P_s}{h\nu B} \tag{3-13}$$

where:

η = detector quantum

P_s = received signal power

B = receiving electronics bandwidth

$h\nu$ = energy per photon

This technique, at unity signal-to-noise ratio, is detection limited only by the quantum photon energy level. The reference signal will beat together with the signal and the noise to convert the signal spectrum down to a lower intermediate frequency, given by:

$$\Delta f = |f_{signal} - f_{reference}| \tag{3-14}$$

A coherent signal derived from a source may contain a frequency component displaced from that of the local oscillator. Detection of this signal by coherent photomixing results in the extraction of this frequency, the detection of this signal being limited only by the signal photon sensitivity and noise sources.

In applying these concepts to optical radar, the Doppler shift that is induced in the laser beam is the result of the velocity component of the target in the direction of the receiver. It is given by:

$$\Delta F_d = \frac{1}{2\pi} (\bar{K}_{sc} - \bar{K}_i) \cdot \bar{V} \tag{3-15}$$

where:

ΔF_d = Doppler shift

$\bar{K}_{sc}$ = preferred scattering direction of beam from target

$= \frac{2\pi}{\lambda_{sc}}$

$\bar{K}_i$ = direction of incident laser beam
$= \frac{2\pi}{\lambda_i}$

λ_i = laser wavelength

$\lambda_{sc} = \lambda_i + \lambda_{Doppler}$

$\bar{V}$ = target velocity relative to transmitter

When receiving such a Doppler signal with a receiver colocated with the transmitter, equation 3-15 reduces to:

$$\Delta F_d = \frac{2\bar{V}}{\lambda_i} \text{Cos } \theta \qquad (3\text{-}16)$$

where:

θ = angle between velocity vector and receiver

When flying into a vortex trail, a laser beam pointed and aligned in the direction of the vortex core will be Doppler Shifted by the axial velocity of the vortex trail, which is small. In order to obtain the largest Doppler shift, the probing laser must be perpendicular to the vortex axis, thus measuring the tangential velocity of the vortex. In any systems deployment of this sensor, the laser beam must scan the vortex over an angular aperture, measuring a component of the resultant vortex velocity distribution in the direction of the receiving telescope.

In order to assess the feasibility of this technique and decide on the desirable laser transmitters that should be used in such a system, the signal-to-noise ratios for detection of the trailing vortex must be

evaluated. The evaluation of such signal-to-noise ratios is necessary to determine the range sensitivity of the system, and independent of the resultant Doppler shifts to be measured.

The theory relates the system signal-to-noise ratio to the laser power, atmospheric parameters, optics diameter, target range, and system bandwidth. The results, shown below, generalized to accommodate a variety of CW and pulsed systems, predict their range resolution and signal-to-noise properties.

The signal-to-noise ratio of coaxial heterodyne backscatter systems is given by:

$$S/N = \frac{\eta P_T \beta(\pi) \lambda}{2Bh\nu} F(R, \lambda, f) \qquad (3\text{-}17)$$

where:

S/N = signal-to-noise ratio

η = photodetector efficiency

P_T = transmitted power, watts

$\beta(\pi)$ = atmospheric backscattering coefficient

λ = laser transmitter wavelength

B = system bandwidth

h = Planck's constant

ν = laser transmitter frequency

$F(R, \lambda, f)$ = resolution function defined in Table 3-III for different coaxial systems

The model used assumes a target a) formed by a diffuse collection of scatterers, randomly distributed, identical and characterized by

Table 3-III. $F(R,\lambda,f)$ Resolution Function

System	F(R, λ, f)
Pulsed-Focused	$\frac{\pi R^2 \Delta L}{\lambda L_{Av}^2}$
Pulsed-Unfocused	$\frac{\pi R^2 \Delta L}{\lambda L_{Av}^2 \left[1 + \left(\frac{\pi R^2}{\lambda L_{Av}}\right)^2\right]}$
CW-Infinite Path-Focused	$\frac{\pi}{2} + \tan^{-1}\left(\frac{\pi R^2}{\lambda f}\right)$
CW-Infinite Path-Unfocused	$\frac{\pi}{2}$
CW-Finite Path-Focused	$\tan^{-1}\left[\frac{\lambda L_2}{\pi R^2} - \frac{\pi R^2}{\lambda f}\left(1 - \frac{L_2}{f}\right)\right] - \tan^{-1}\left[\frac{\lambda L_1}{\pi R^2} - \frac{\pi R^2}{\lambda f}\left(1 - \frac{L_1}{f}\right)\right]$
CW-Finite Path-Unfocused	$\tan^{-1}\left(\frac{\lambda L_2}{\pi R^2}\right) - \tan^{-1}\left(\frac{\lambda L_1}{\pi R^2}\right)$

where:
- R = radius of transmitter telescope
- λ = wavelength
- ΔL = length of resolved scattering volume
- L_{AV} = average range-to-scattering volume, $L_{AV} >> \Delta L$
- L_1 = distance to beginning of scatter path
- L_2 = distance to end of scatter path
- f = location of focus

the atmospheric backscattering co-efficient $\beta(\pi)$, b) where all particles in the scatter volume have the same average velocity relative to the transmitter-receiver and hence will manifest at any given time a single Doppler shift, c) where loss of coherence due to the propagation of the beam from the transmitter back to the receiver is much smaller compared to the diffuse nature of the target. The equations that are presented in Table 3-III have been programmed for the pulsed and CW focused and unfocused systems.

The far-field distance, approximately given by $\pi R^2/\lambda$, where R is the radius of the receiver optics, determines whether a focused or unfocused CW or pulsed system configuration should be used in the remote measurements. A general conclusion[20] is that in either case, a focused system performs with a resultant higher signal-to-noise ratio in the near field, for far-field operation the difference between the systems being less than 3 dB.

The above theory and resultant equations have been applied to the design and operation of CW and pulsed CO_2 laser, 10.6 micron wavelength optical radars. Let us briefly review some of the salient systems and hardware developments in 10.6 micron optical Doppler radars to-date, before evaluating the feasibility of using such systems in the airborne detection of vortices.

3.2.2.2 CO_2 Laser Doppler Radar Developments for Atmospheric Measurements

A one-dimensional laser Doppler remote atmospheric wind measure- system has been developed and evaluated by the Raytheon Company for

the NASA Marshall Space Flight Center in Huntsville, Alabama.[15] The system (Figure 3-7), consists of a 20-watt monochromatic CO_2 laser, whose output is coupled through the interferometer and optically focused by a 6-inch telescope. The range to which the laser beam is focused is determined by a calibrated adjustment control on the telescope. The resultant backscattered energy from atmospheric particulates is then collected by the same telescope and directed through the interferometer to a copper-doped germanium detector operating at $4^{o}K$. After passing through suitable receiver electronics a Doppler frequency corresponding to the motion of the natural aerosols is observed in realtime on a spectrum analyzer.

During a field test program conducted at Colorado State University in Fort Collins, Colorado, measurements were made under a variety of atmospheric conditions. Photographs taken of a spectrum analyzer display, shown in Figure 3-8 , illustrate the atmospheric velocity vector along the laser beam propagation path of 40 - 56 KM per hour (25 - 35 mph) consistent with the component of wind velocity being monitored.

Additional measurements made during a snow storm at several ranges from 33 meters (100 feet) to 525 meters (1,600 feet) by adjusting the optical focus of the system are illustrated in Figure 3-9 . Here the horizontal axis corresponds to wind velocities from 0 to 38.5 KM per hour (24 mph) and the vertical scale provides an indication of the signal strength. Figure 3-9 also illustrates the system noise in the absence of a signal.

A similar system has been applied to the detection of aircraft trailing vortices. Figure 3-10 illustrates the test set-up.

In order to obtain a visualization of the vortex pattern generated, a smoke bomb was elevated to the top of the tower. A typical run

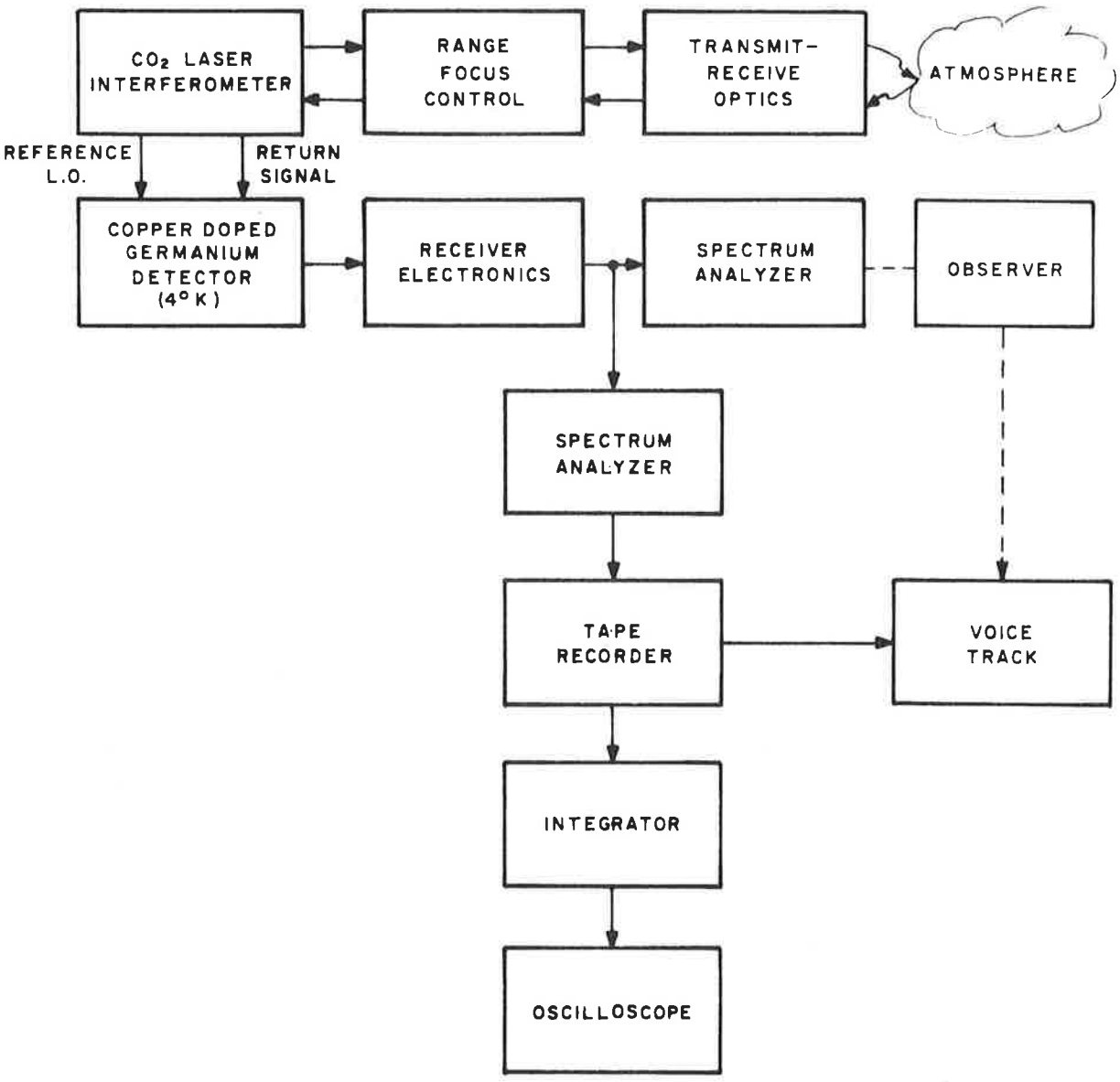

Figure 3-7. Laser Doppler Velocimeter Block Diagram

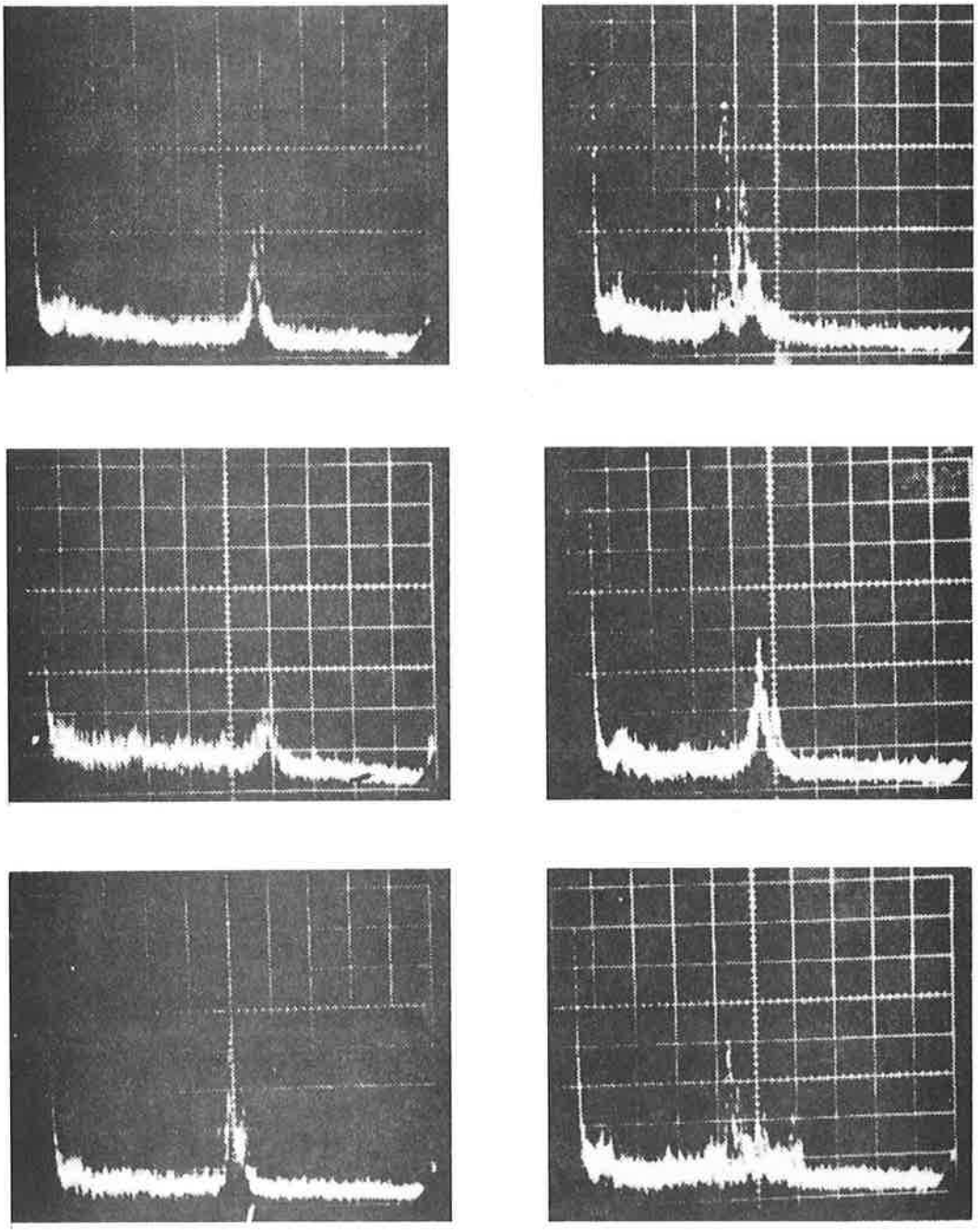

GROUND WIND RETURNS, FT. COLLINS, COLORADO, MARCH 31, 1971

0.5 MHz PER DIVISION
5 MHz FULL SCALE
60 MILES PER HOUR FULL SCALE

Figure 3-8.

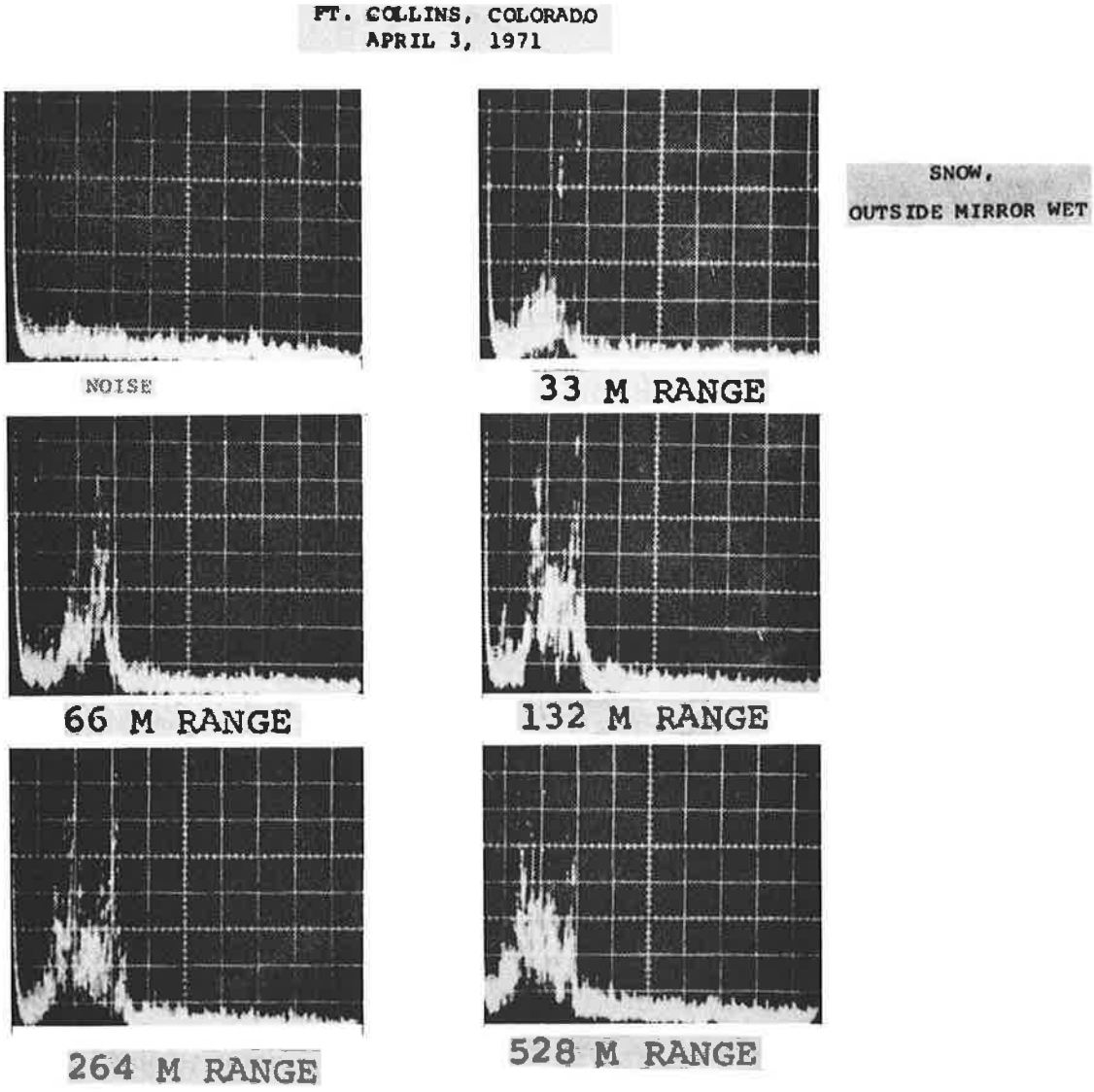

Figure 3-9. Ground Wind Returns on CW Focused LDV System

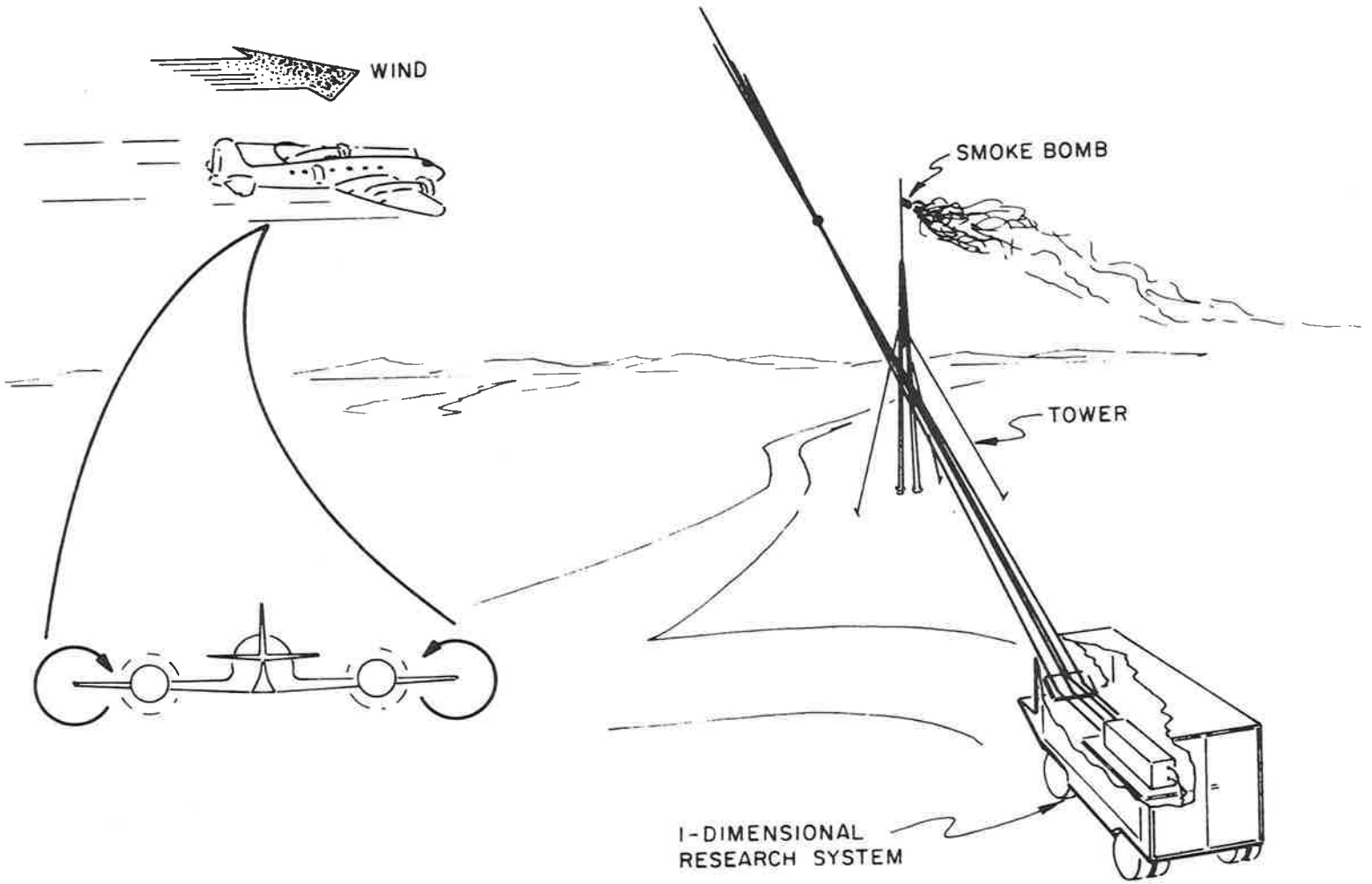

Figure 3- 10. Experimental Field Test Arrangement

consisted of the test aircraft being directed by radio contact, flying at 40 feet altitude up-wind of the tower. The laser Doppler velocimeter was then focused 80 feet from the test van and approximately 10 feet up-wind from the tower. In this test configuration the vortex is detected by the laser system prior to being visualized, as shown in Figure 3-11, by the smoke being entrained in the vortex.

The remote measurement of wind speed and wind speed fluctuation is typically monitored by viewing the CRT display of a spectrum analyzer having a full scale frequency of 1.5 MHz, corresponding to a velocity of 26 FPS. Typical examples of the remote atmospheric wind signal observed on this analyzer may be noted in Figure 3-12.

The C-47 E test aircraft utilized during these tests has the following specifications:

Gross weight -- 11,800 KG (26,000 lbs.)
Wing span -- 31 Meters
Velocity -- 100 Knots

and its expected core velocity is 8 M/Sec (24.2 Ft/Sec). From Figures 3-12C and 3-12D, vortex core velocities of this magnitude are measured on the display as the vortex passes through the propagation path.

The sequence of photographs in Figure 3-12 represents the vortex velocity within the resolution volume of the laser Doppler radar during the traverse of the vortex. Figures 3-12A and 3-12G represent conditions before and after vortex traversal and correspond to ambient wind velocity distributions. As the laser beam enters the vortex the peak velocity increases (Figure 3-12B). Figures 3-12B, C, D, E, and F show the velocity distribution as the laser beam approaches and recedes from the core. After the vortex leaves the laser beam, the

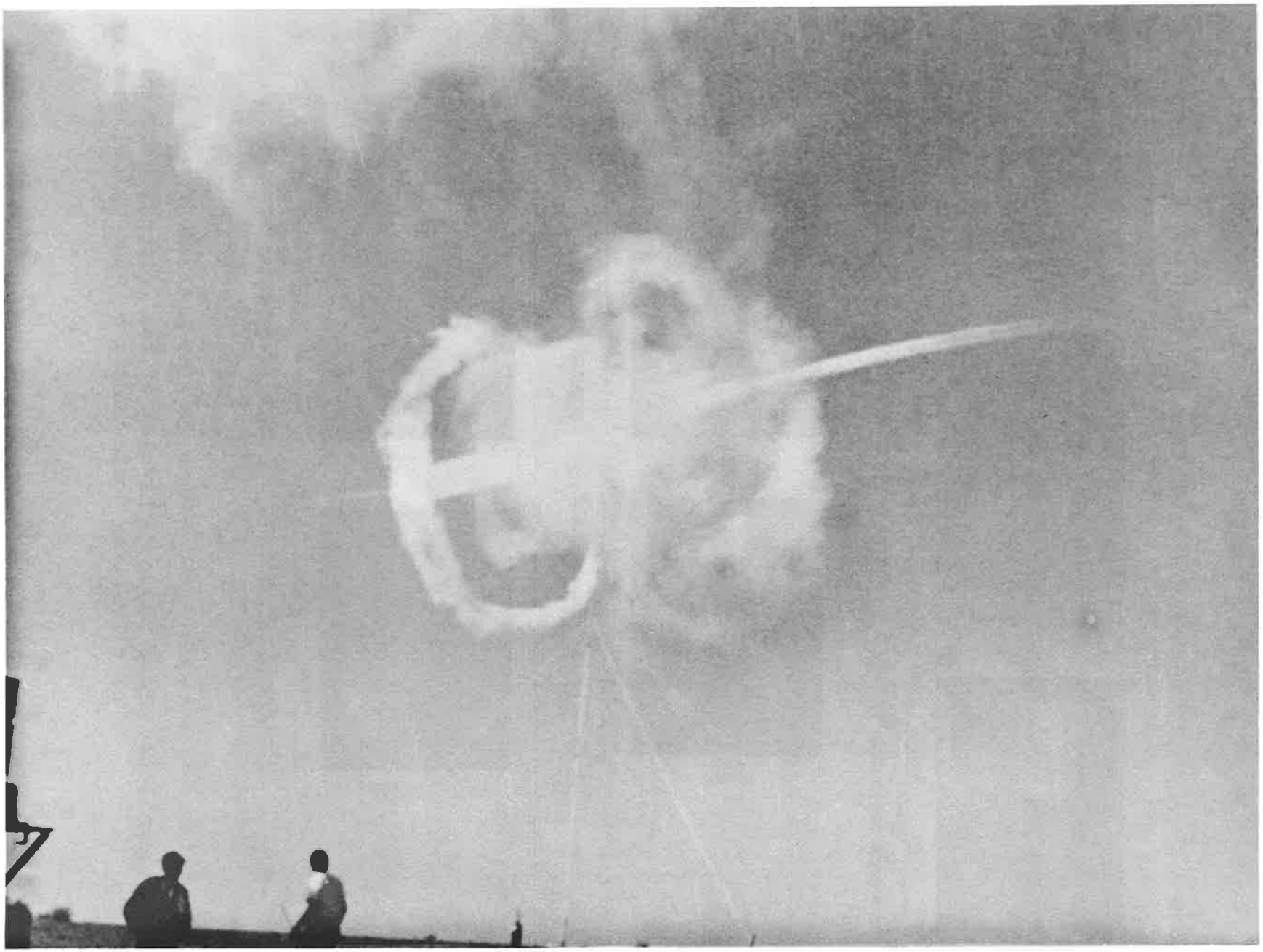

Figure 3-11. Vortex Visualization in LDV Experiment

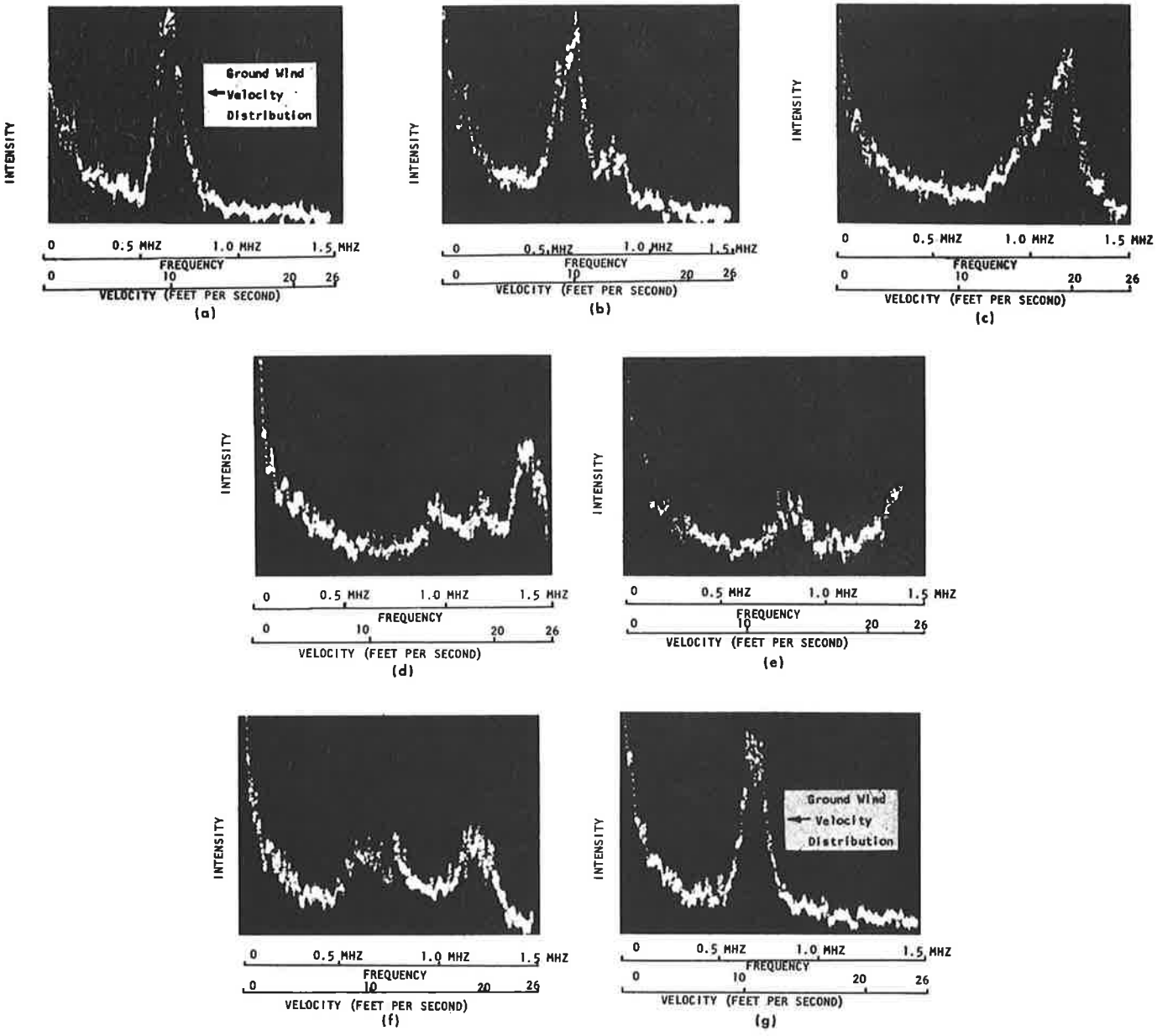

Figure 3-12. Time Sequence Display of the Velocity Structure of a Trailing Vortex Using a Laser Velocimeter.

wind signature returns.

The above are examples of the application of CW Doppler techniques to the measurement of atmospheric motion. More pertinent to our interest herein for the in-flight detection of vortices is the very recent work performed by the Raytheon Company, Sudbury, Mass. in the development of a flyable pulsed Doppler CO_2 laser radar system for the detection of clear air turbulence.(16)

The system consists of a coherent laser radar transmitter on an airplane, radiating 2 to 10 microsecond wide pulses. These pulses are scattered by the aerosols in the turbulent area, shifting in frequency by the motion of the turbulent air to produce a Doppler change or modulation in the returning pulse. The time of return of the pulse indicates the distance away from the disturbance, and the Doppler changes, by revealing the velocity variations within the turbulent region, indicate the intensity of the turbulence.

A series of flight tests conducted in 1972 aboard the NASA Convair 990 flight test aircraft have indicated the flight worthiness of the instrument and its ability to remotely measure atmospheric turbulence at low altitudes. Figure 3-13 illustrates a range-velocity presentation of a wind shear occurring along a 5 N.Mi. path in front of the NASA aircraft flying over a dust storm.

Additional measurements have been obtained from clear air, clouds, and ice crystals at a variety of ranges and altitudes. Present efforts are directed at improving the system's sensitivity to detect high altitude wind speed and turbulence by improving the system sensitivity and performing the post-flight data analysis to determine atmospheric scattering cross-section, equipment performance and turbulence correlation. Future efforts must be directed toward size and weight reduction of the instrument for its commercial utilization.

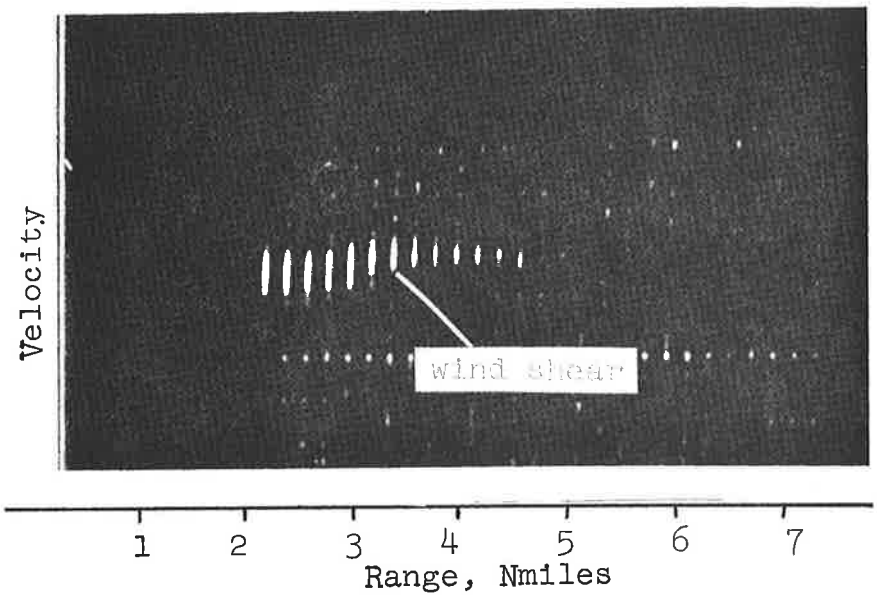

Figure 3-13. Range-Velocity Display During Flight Over Dust Storm

Figure 3-14 shows how the anticipated Doppler/range return, suitably processed, could be displayed on the aircraft weather radar screen. By sensing the Doppler spread, the instrument locates the turbulent areas of dangerous intensity and provides data for the aircraft by which the pilot may avoid an encounter with clear air turbulence. Such measurements, still in progress, have been made over several miles at altitudes ranging from a few to tens of Kilofeet. A similar application of the system to wake vortex measurements will be shown to be feasible.

3.2.2.3 Detection of Trailing Vortices

The distribution of tangential velocities that may be expected from vortices shed from the more typical airplanes ranges from 100 ft/sec to 200 ft/sec. At 10.6 microns, a Doppler shift of about 60 kHz/ft/sec is expected for the case where the incident laser beam is perpendicular to the core of the vortex. Hence, typical 100 ft/sec to 200 ft/sec tangential vortex velocities will yield Doppler shifts of 6 MHz to 12 MHz. However, the airplane whose laser sensor is scanning the airspace below its own altitude or to the side of it will interact with the vortex at a line-of-sight angle, thus reducing the above values to much lower levels, as calculated by Equation 3-16. For an aircraft directly in the line-of-sight of the first, the contribution of the axial velocity component may be of the order of 5 ft/sec to 20 ft/sec, resulting in Doppler shifts of 300 kHz to 1.2 MHz. When designing such an optical radar system, the receiver electronics can accommodate and display this distribution of Doppler shifts.

An optical laser radar that scans the airspace below and to the side of it may observe a vortex signature in terms of a frequency spectrum or an ensemble of individual velocity components appropriately displayed as a function of range. Let us now evaluate the signal-to-noise ratios as a function of range for a pulsed CO_2 laser radar system.

WEATHER RADAR AND TURBULENCE DISPLAY

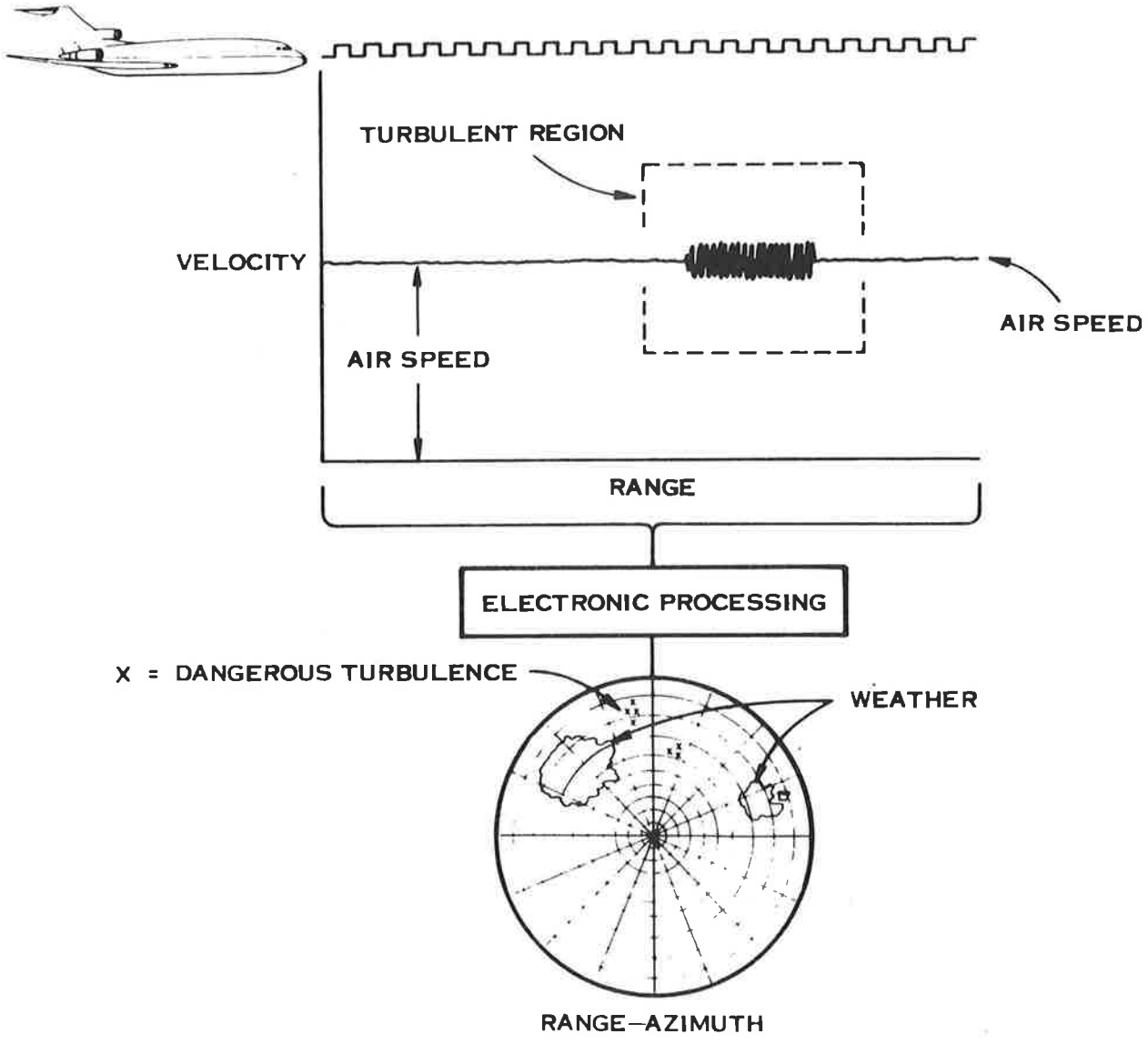

Figure 3-14.

This calculation is independent of the Doppler shifts to be measured by the system. We shall assume that the Doppler radar has the following parameters:

Type of system	Pulse unfocused
PRF:	200 sec^{-1}
Laser average power:	5 watts
Pulse duration:	10 microseconds, 4 microseconds
Diameter of receiver optics:	2", 4", 6", 12", 18"

We assume that the aerosols in the atmosphere, entrained by the vortex are primarily responsible for providing the backscattering cross-section for the 10.6 micron laser pulses. The backscattering coefficient that has been used in these computations is altitude dependent and given by

$$\beta(\pi) = 10^{-4} \text{ km}^{-1}$$

with its value decreasing by 8 dB for each 10 kft. increase of altitude. This is a recently experimentally determined value[21] that reflects reasonably well the atmospheric conditions under good weather conditions. The equations represented in Table 3-III in Section 3.2.2.1 have been evaluated.

Figures 3-15 and 3-16 indicate the results obtained. A 4" diameter, 5 watt, 10 microsecond, 200 pulses/sec transceiver will detect the presence of a vortex trail, on single pulse returns, over a distance of 5 miles at altitudes ranging from 500 ft. to 5,000 ft. with a SNR of about 13 dB. The size of the vortex trail sampled by the pulsed system is about 4500 feet. A 6" diameter transceiver, with a 5 watt CO_2 laser, 4 μsecond pulse width, yields at 5 miles, on single pulse detection, a SNR of 16 dB. Larger diameter transceivers do not improve the SNR.

3.2.3 RAMAN LIDAR AND OTHER SPECTROSCOPIC TECHNIQUES

The incoherent detection Lidar technique, using Ruby or Nd:YAG lasers, and the Doppler optical radar, using a CO_2 laser, both depend

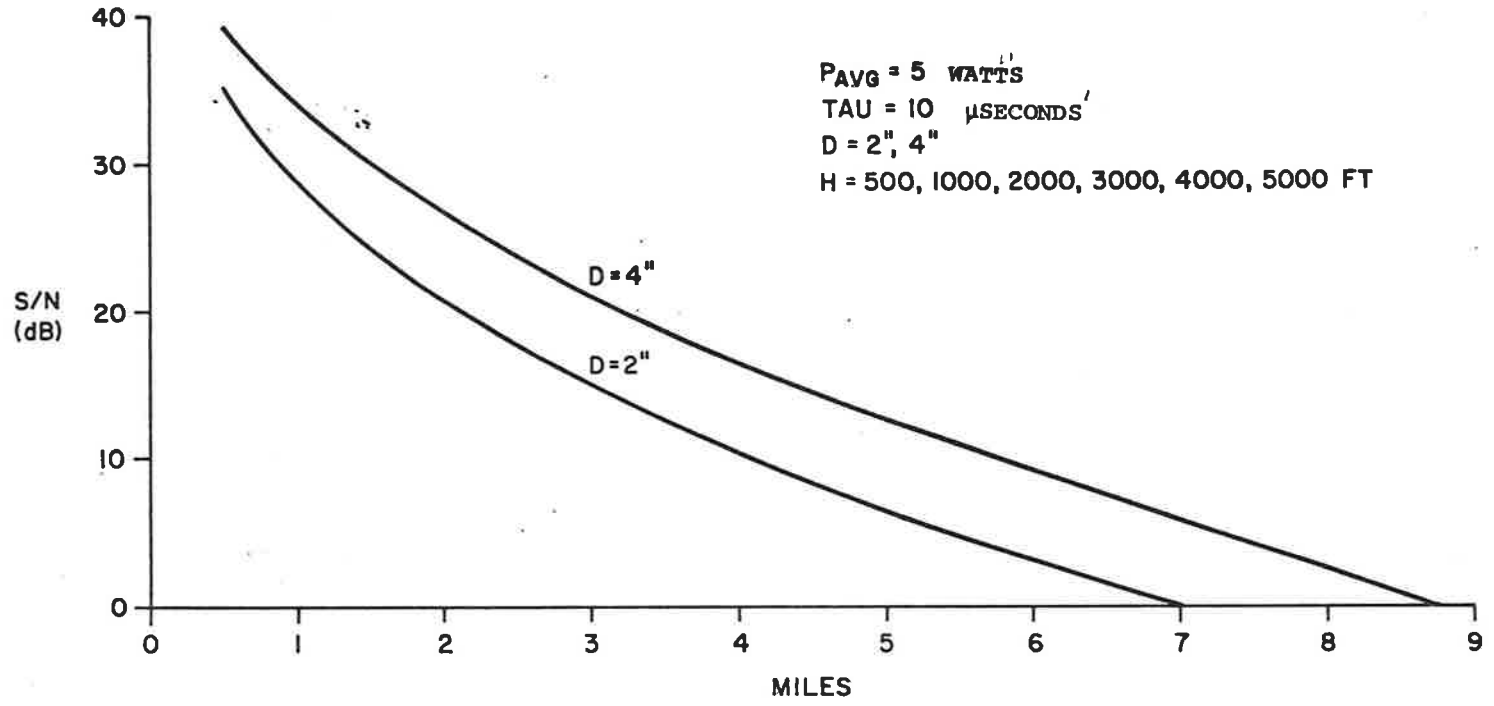

Figure 3-15. SNR vs. Range to 5000 ft. on 2" and 4" Diameter System.

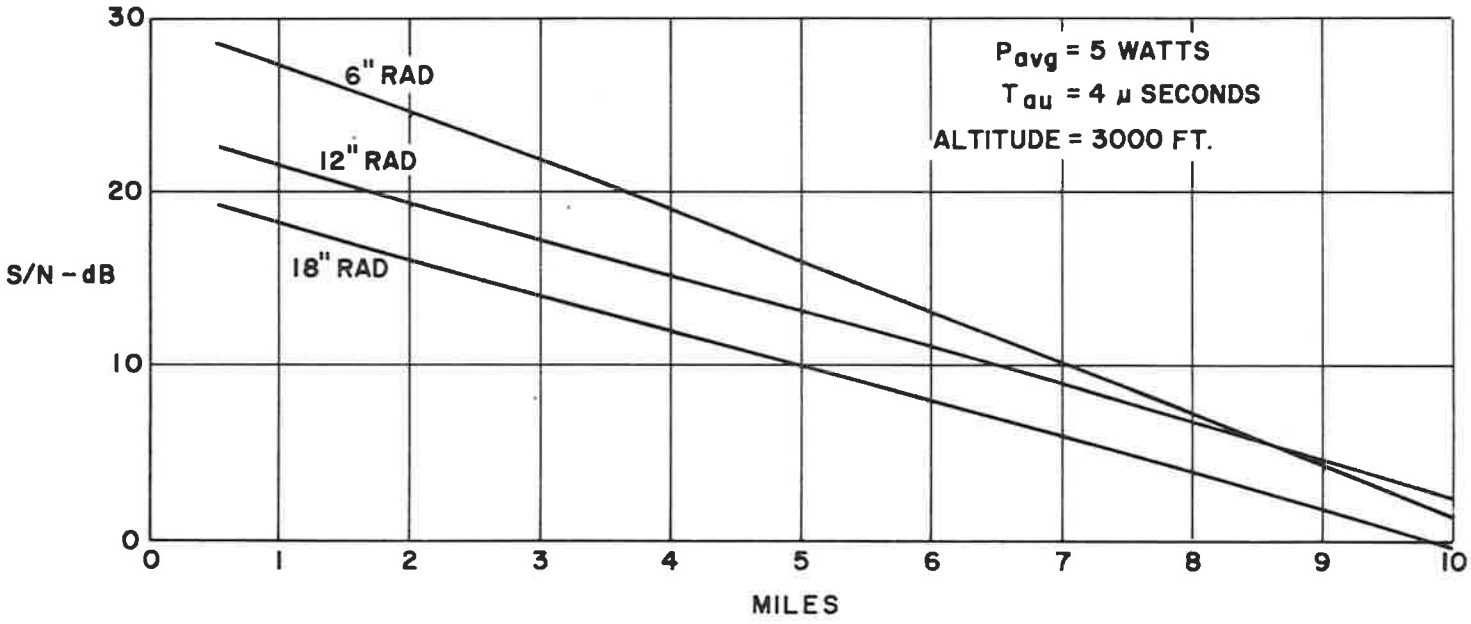

Figure 3-16. SNR vs. Range to 3000 Ft. on 6", 12" and 18" Diameter System

on backscattering from particulate matter in the vortex wake. This particulate matter is entrapped in the vortex from emissions of the engines and atmospheric aerosols. The gaseous exhaust constituents of the engines, for instance N_2, H_2O vapor, CO_2 and hydrocarbons have the largest volumetric concentrations and diffuse out into the wake. For engines located on the wings, as for instance the B-707, B-747, DC-10, L-1011, exhausts may find their way into the vortex trail. Very recent measurements[22] to detect the presence of water vapor in the vortex trail have confirmed this hypothesis. On the other hand, aircraft whose engines are mounted at the tail-end of the plane, for instance the B-727 and DC-9, may not see their engine exhausts diffuse out into the vortices. The whole subject matter of diffusivity of the engine emissions into the vortex, the distances behind the airplane where such mixing occurs is still not well founded in fact. Theoretical models of the phenomenology are not as yet available. It seems, nevertheless, important to identify the processes by which the presence of these exhausts may be determined.

Three spectroscopic approaches avail themselves: absorption, emission, fluorescence scattering and re-emission processes. We consider these processes in the frequency range from the near ultra-violet to the far infrared. In the Lidar and Doppler optical radar techniques that were examined in Sections 3.2.1 and 3.2.2, the fundamental mechanism yielding a backscattering cross-section was Mie-scattering. In this type of process, the interaction is between particles of a size commensurate with the wavelength of the electromagnetic radiation. In the processes to be considered, the interaction mechanism operates at the molecular and atomic levels.

Fluorescent scattering occurs only when the frequency of the incident radiation is in an absorption line or band in the sample material. Transition to a state of higher energy may occur, followed by relaxation and emission of light at frequencies equal to or less than the

incident frequency. The emitted and absorbed radiation frequencies are dependent on the detailed structure of the molecular energy level diagram and hence are characteristic of the molecule. Figure 3-17 is a spectra in the near infrared region of the absorption characteristics of many of the exhaust products found in jet engine emissions.

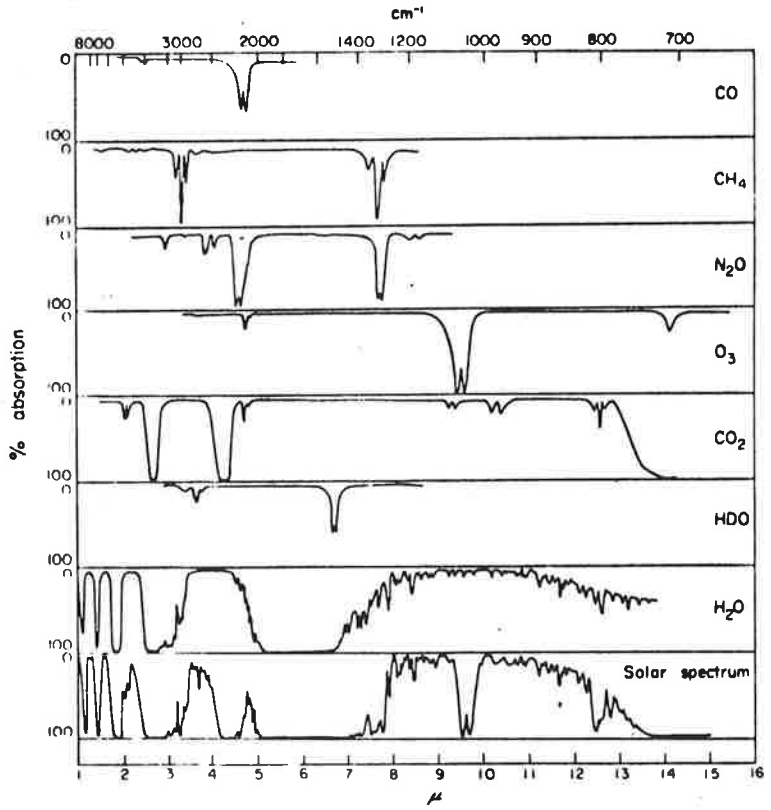

Figure 3-17. IR Absorption Spectra

To induce fluorescence scattering in the vortex trail containing the jet engine exhaust it is necessary to illuminate the sampled region with a laser of the correct wavelength. In recent work performed[23] with a turbine exhaust simulator burning JP-4, large optical signals, presumably from unburned hydrocarbons, have been observed by scattering produced by a 3371 Å pulsed nitrogen laser. The effective cross-section of the interaction was observed to be 10^7 to 10^6 larger than the N_2 Raman cross-section; i.e., of the order of 2.0×10^{-23} cm^2/ster. This is clearly an indication of a resonance or fluorescence type process going on in the detection of the hydrocarbons. This work has been performed on a turbine-engine test bed, and thus the findings do not apply to in-flight measurements. However, the feasibility of performing the same measurements in-flight, detecting hydrocarbon effluents in the wake should be investigated.

Emission from the vibrational-rotational transitions of water vapor lines in the 8-micron to 14-micron range has also been recently observed, about $2\frac{1}{2}$ miles behind a plane, from in-flight measurements of the vortex trail.[22] Figure 3-18 is a plot of the raw-data as obtained with a Barnes PRT 5 radiometer, at an altitude of 33,000 ft. The sketch shows the flight formation.

Raman scattering, although the weakest of the spectroscopic emission phenomena to be considered, is useful because it occurs regardless of the irradiating frequency. The radiation frequency need not be matched with molecular resonances to allow transitions of the molecule. This is not so in fluorescence scattering, since the laser emission frequency must match the absorption frequency of the molecules. Hence, in this case, tunable laser sources are required. The recent work reported in Reference (23) above, does match the 3371 Å emission wavelength of the N_2 laser, to one of the absorption line of jet

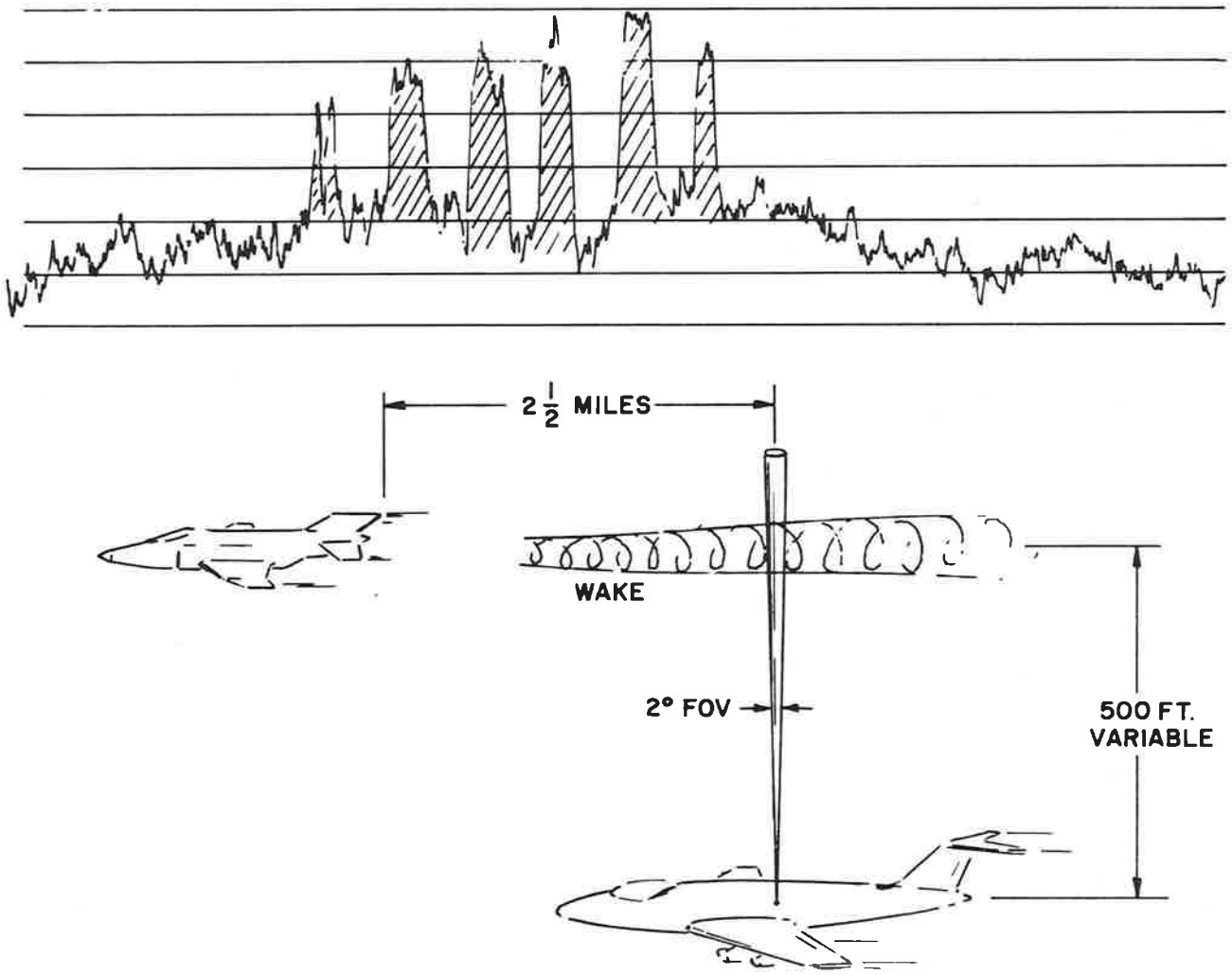

Figure 3-18. Passive Detection of Wake in the 8 Micron to 14 Micron Range With Barnes PRT-5 Radiometer at an Altitude of 33,000 Ft. (22)

exhaust hydrocarbons. In Raman scattering, if the incident radiation is at frequency ν, Raman lines occur at a series of frequencies $\nu \pm \nu_1$, $\nu \pm \nu_2$, etc. Table 3-IV is a compilation of Raman cross-section data for species of interest, in the ultra-violet range of wavelengths[24]. Thus, unlike Mie-scattering, the spectral return of the Raman or fluorescence scattering is specific to the molecules interacting with the Lidar radiation, and can be used as a means of identifying the presence of engine exhaust products, hence the existence of the wake, behind an aircraft. Figure 3-19 shows the number of signal photons as a function of range for several of the engine exhaust products, N_2, O_2, H_2O, CO_2, N_2O and NO.[25] The sky background noise, under various conditions of interest, appears on the left side and detector dark noise from selected photomultipliers appears on the right side of the scale. The Raman wavelengths of the exhaust species of interest are found in Table 3-IV. The transmitter and receiver parameters are as given:

Transmitter:

Peak power:	100 kW
Pulse width:	10×10^{-9} seconds
Wavelength:	3371 Å
PRF:	100 pps

Receiver:

Diameter:	25 cm
Filter bandwidth:	10 Å
Optical efficiency:	75%
Detector quantum efficiency:	18%
Range resolution:	10 meters
Number of pulses integrated:	1

The number of photoelectrons received is from a range increment of

TABLE 3-IV.

RAMAN CROSS SECTION DATA FOR SPECIES OF INTEREST

Molecule	Vibrational Energy Spacing	Wavelength of Raman Scattering With 3371 Å Laser Source	$\frac{\sigma_{RAMAN}}{\sigma_{RAMAN(N_2)}}$		Absolute Cross-section
SO_2	1151 cm^{-1}	3507 Å	2.4	(A)	4.8×10^{-30} cm^2/ster
CO_2	1286	3524	2.2	(B)	4.4×10^{-30}
	1388	3537	2.2		4.4×10^{-30}
O_2	1556	3558	1.5	(C)	3.0×10^{-30}
NO_2	1621	3566	not available*		
H_2CO	1744	3582	not available*		
NO	1876	3599	0.5	(D)	1.0×10^{-30}
CO	2143	3634	2.0	(E)	4.0×10^{-30}
N_2	2330	3658	1.00		2.0×10^{-30}
CH	2920 (average)	3740	10	(F)	2.0×10^{-29}
H_2O	3652	3844	4.2	(G)	8.4×10^{-30}

(A), (D) Leonard, D. A., J. Appl. Physics 41, 4238 (1970).

(B) Derr, V., Wave Propagation Laboratory, NOAA, Boulder, Colorado, Private Communication

(C) Widhopf and Ledermann, Polytechnic Institute of Brooklyn, Report No. 69-46.

(E), (F) Leonard, D. A., Unpublished results at AERL.

(G) Cooney, John, Drexel Institute of Technology, Private Communication.

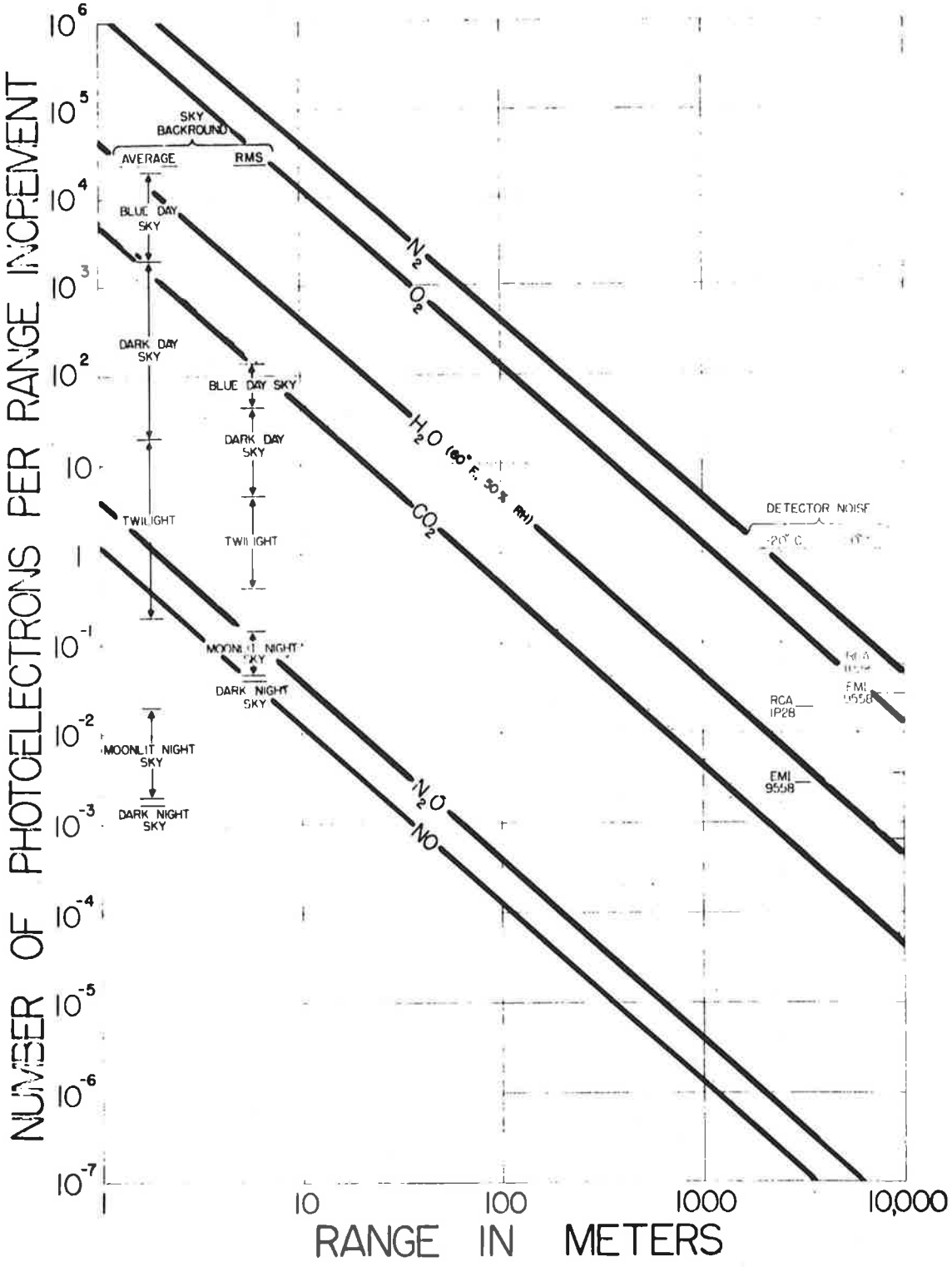

Figure 3-19. Raman Signal vs. Range with Background and Detector Noise Magnitudes (25)

1.5 meters. Using a cooled detector, a SNR of 30 dB is obtainable at a range of 100 meters from the Raman shift of water vapor. It can be ascertained that this technique, useful as it is, will be limited to the detection of engine exhaust products over short ranges of a few hundred meters.

3.3 ACOUSTIC RADAR

In a backscattering configuration, the differential scattering cross-section of acoustic radiation interacting with an isotropic turbulent medium is given by[26]:

$$\frac{d\sigma(\pi)}{d\Omega} = 2\pi K^4 \, V \, \frac{\Phi_T(2K)}{4T^2} \qquad (3\text{-}18)$$

where:

$\frac{d\sigma(\pi)}{d\Omega}$ = differential acoustic scattering cross-section for backscattering

K = $\frac{2\pi}{\lambda}$, acoustic wave number

$\Phi_T(2K)$ = 3-dimensional temperature spectral density

T = absolute temperature within scattering volume

V = scattering volume

The concepts brought forth in Section 3.1.1.2 on the structure function of refractivity $D_n(r)$, structure function parameter C_n, and their relationship to $\Phi_T(2K)$, the spectral intensity of the fluctuations, are also valid at acoustic wavelengths. As shown in Table 3-V,[25] comparison of the C_n's for acoustic, radio and optical waves indicates that for isotropic turbulence and typical atmospheric irregularities the radar cross-section which is a function of C_n^2 as shown in Equation 3-4, will be several orders of magnitude larger for acoustic waves than for radar or optical waves. In a backscattering configuration, the acoustic radar will only sense the fluctuations in the

Table 3-V. Relative Values of Atmosphere Structure Function Parameter, C_n, for Acoustic, Radio and Optical Waves

Atmospheric Condition ΔR = 1 metre	Acoustic $C_n \times 10^6$	Radio $C_n \times 10^6$	Optical $C_n \times 10^6$
Δ_T^{RMS} = 1°K	1720	1.26	0.93
Δ_E^{RMS} = 1 mbar	138	4.50	0.04
Δ_V^{RMS} = 1 m/sec	0-4000	2×10^{-6}	2×10^{-6}

vortex due to temperature discontinuities in the wake. Such measurements will indicate, within good levels of confidence, the existence of the wake because the temperature gradients radiating from the engine are known to exist over several miles behind the airplane. Thus, the use of the acoustic radar will identify the presence of the vortex due to a signature derived from the convection and radiation of heat into the wake.

Studies performed on bistatic, CW Doppler[27] and pulsed acoustic radars[28], have shown promise of their applicability in ground-based vortex detection systems at airports. However, by virtue of the finite propagation velocity of sound, 1000 ft/second at NTP, an airplane traveling at 400 ft/sec will have traveled a distance of 20,000 ft. during the time that it will take an acoustic pulse to propagate out to a distance of 5 miles and return back to the radar. Thus, the effective distance over which such a measurement takes place is 30,000 ft., or about 3 miles out from the airplane.

The selection of an active acoustic probe operating in a monostatic, backscattering configuration is ultimately determined by S/N ratio available at the receiver terminal. Experience to date with ground-based monostatic acoustic systems is only now developing. The operation of an airborne system may be determined only after the noise contributions generated by boundary layers around the aircraft fuselage, wind and environmental noise, and jet engine noise have been evaluated. These and determination of the acoustic backscattering cross-section as a result of temperature fluctuation in the vortex generated turbulence is presently unknown. On-going work on acoustic ground-based systems may shed further light on the highly speculative differential cross-section, thus enabling reasonable estimates of this system application to be performed in the future.

3.4 PASSIVE ULTRA-VIOLET MEASUREMENTS

The use of active UV lasers in exciting fluorescent emission or inducing Raman shifts in the molecular signature of various engine exhaust constituents has been reviewed and its feasibility over short distances, of the order of a few hundred meters, established. Recent work performed has tried to establish the presence of such UV emissions from naturally occurring transitions in Nitric Oxides at the exhaust port of aircraft engines. The technique, a photographic one, developed for airborne terrain studies and atmospheric research, has shown some results as a possible remote detector and monitor of nitric oxide, one of the oxides of nitrogen that is a critical pollutant in jet aircraft engine exhaust. The research seems to indicate that ultraviolet reconnaissance appears capable of isolating the nitric oxide signature in engine emissions [29,30] during daytime light conditions.

Initial studies of engine emissions have produced a characteristic spectral signature of particulate matter that ultraviolet photography can capture. Thus particulate matter and pollutants not visible under normal viewing conditions have the same appearance on UV pictures as visible smoke has on conventional photographs. Several photographs of aircraft during takeoff and climbout using this technique have shown the otherwise invisible trailing plumes that are sucked into the pattern of the two wing-tip vortices.

The technique has shortcomings because it is slow, requires the development of the film, and does not lend itself to a real-time video display system. Though useful for ground-based research measurements, the ultraviolet reconnaissance technique is presently not feasible as an airborne instrumentation system for detecting vortices.

Further investigations of the passive detection of nitric oxide emissions in the UV band should be pursued with more sensitive

photodetectors rather than UV photographic film. This technique, with sufficiently sensitive detectors, may lend itself to the determination of the presence of a vortex trail since NO and NO_2 emissions, resulting from the heating of the air by the jet engine exhaust, are of a sufficiently high, 50 to 400 PPM, concentration. However, by its very passive nature it may be limited to very short ranges. Passive instrumentation, whether UV or IR, will be less expensive to develop or use than any equivalent electro-magnetic wave active probe. However, the effectiveness of the UV technique can only be determined when more quantitative measurements are obtained and evaluated.

REFERENCES - SECTION 3

(1) RDR-IE/ED Airborne Weather Radar System, Equipment, Installation and Operation Manual, Bendix Avionics Division, Bendix Corporation, June 1968.

(2) Weather Radar by Bendix - The Weathervision System, p. 23, "Electronics News", October 9, 1972.

(3) Aircraft Wake Vortex Sensing Systems, Annual Report, June 30, 1971, DOT-TSC.

(4) Handbook of Geophysics and Space Environments, Chapter 5, AFCRL, McGraw Hill Book Co., 1965.

(5) Easterbrook, C. C., and Joss, W. W.: " The Utility of Doppler Radar in the Study of Aircraft Wing-tip Vortices", p. 97, Proc. of a Symposium on Aircraft Wake Turbulence, Seattle, 1970, Plenum Press, N. Y., 1971.

(6) Hardy, K. R.: "Studies of the Clear Atmosphere Using High Power Radar", Remote Sensing of the Troposphere Symposium, ed. by V. Derr, University of Colorado, Summer 1972.

(7) Hardy, K. R., and Katz, I.: "Probing the Clear Atmosphere with High Power High Resolution Radars", Proc. IEEE, p. 468, April 1969,

(8) Tatarski, V. I.: Wave Propagation in a Turbulent Medium , McGraw Hill Book Co., New York, N. Y., 1961.

(9) Ottersten, Hans: "Atmospheric Structure and Radar Backscattering in Clear Air", Radio Science, pp. 1179-1193, Vol. 4, No. 12, December 1969.

(10) The NASA Marshall Space Flight Center and NASA Ames Research Center have continuing programs to study vortex structure in wind tunnels using laser Doppler techniques.

(11) Okean, H. C., and Lombardo, P. P.: "Noise Performance of M/W and MM-Wave Receivers", The Microwave Journal, pp. 41-50, January 1973.

(12) Skolnik, M.: Introduction to Radar Systems , Chapter 11, McGraw Hill, 1962.

REFERENCES - SECTION 3 (continued)

(13) Communication from Dr. Hector Ingrao, DOT/TSC, Cambridge, Mass.

(14) Hinkley, E., Kelley, P. L.: Science 171 (1971), pp. 635-639.

(15) Jelalian, A., Keene, W. H., Sonnenschein, C. M., and Huffaker, R. M.: "Laser Doppler Systems for Remote Atmospheric Measurements", NEREM, Boston, Mass., November 1971.

(16) Raytheon Company, Electro-Optics Department, Sudbury, Mass., work performed for the NASA/MSFC under Contract No. NAS 8-28424.

(17) Huffaker, R. M., Jelalian, A. V., and Thomson, A. F.: "Laser Doppler System for Detection of Aircraft Trailing Vortices", Proc. IEEE, Vol. 58, #3, March 1970.

(18) Fuller, C. E.: "Wing Tip Vortex Measurements", RTR 002-3, RemTech Corporation, Huntsville, Ala., Final Report on Contract NAS 8-25896, April 1973.

(19) Orloff, K. L., Grant, G. R.: "Application of a Scanning Laser Doppler Velocimeter to Trailing Vortex Definition and Alleviation", AIAA 6th Fluid and Plasma Dynamics Conference, July 1973. AIAA Paper No. 73-680.

(20) Sonnenschein, C. M., and Horrigan, F. A.: "Signal-to-Noise Relationships for Coaxial Systems that Heterodyne Backscatter from the Atmosphere", Applied Optics, Vol. 10, p. 1600, July 1971.

(21) Communicated by D. A. Kawachi, Raytheon Company, Sudbury, Mass.

(22) Private Communication from Robert Muñoz, NASA Ames Research Center, Moffett Field, Cal.

(23) Private Communication from D. A. Leonard, Avco-Everett Research Laboratory, Everett, Mass.

(24) Leonard, D. A.: "Development of a Laser Raman Aircraft Turbine Exhaust Emissions Measurement System", Research Note 914, May 1972, Avco-Everett Research Laboratory, Everett, Mass.

(25) Derr, V. E., and Little, C. G.: "A Comparison of Remote Sensing of the Clear Atmosphere by Optical, Radio and Acoustic Radar Techniques", Applied Optics, Vol. 9, No. 9, p. 1976, September 1970.

(26) Kallistratova, M. A.: "Experimental Investigation of Sound Wave Scattering in the Atmosphere", Trupy Inst. Fiz. Atmosfery, Atmosfernaye Turbulentmost, No. 4, pp. 203-256, 1971.

(27) Balser, M., Nagy, A. E., McNary, C.: "Acoustic Analysis of Aircraft Vortex Characteristics", FAA Report FAA-RD-72-81, July 1972.

(28) Sullivan, T., Burnham, D., Kodis, R.: "Vortex Sensing Tests at Logan and Kennedy Airports", TSC Report No. FAA-RD-72-141, December 1972.

(29) Michanowsky, George: "The Potential of UV Reconnaissance as a Remote Detector of Invisible Nitric Oxide", Amazonia Foundation, Box 651, New York, N. Y., September 1971.

(30) Michanowsky, George: "UV Reconnaissance as a Remote Detector and Tracker of Wake Turbulence", Amazonia Foundation, Box 651, New York, N. Y., November 1972.

SECTION 4

CONCLUSIONS

Any large aircraft, for instance a L-1011, DC-10 or B-747, extensively used at airports open to transportation or general aviation traffic, creates a hazardous situation at landing or take-off by generating strong vortices with a time constant larger than the aircraft spacing intervals. The determination of vortex intensity and location is being planned through the use of ground based detection and prediction systems, that can forewarn air traffic control of the existence of these vortices. However, a strong case can be made for the measurement of vortex location and intensity from in-flight instrumentation platforms, enabling each aircraft, small or large, to determine on its own the presence of vortex trails which may be in its path of flight. Such measurements will help pilots flying on VFR to prelocate any vortex turbulence region in the vicinity of the airport, and thus either accelerate or retard their approach to the runway. Needless to say, such a system will supplement a ground-based vortex detection instrumentation system at large airports, while providing prime inputs to smaller airports, which also have a vortex hazard situation.

It has been shown, in this study, that a modification of the front-end receiver of a presently on-board 10 GHz weather radar system; or a change of frequency to 35 GHz, may result in the feasibility to obtain vortex identification information over a range of several kilometers. The parameter of importance in this assessment, which is not presently known with confidence, is the equivalent radar cross-section presented by the vortex. Recent work reported at the 15th Weather Radar Conference that met in Urbana, Illinois in October 1972, has indicated that

for the first time the presence of aircraft trailing vortices has been detected by radar. This, in itself, is encouraging and supports our conclusion that a practical feasibility study of this technique and system should be undertaken.

The CO_2 laser coherent Doppler radar technique will definitely detect the presence of the trailing vortex over a range of at least 5 miles, when a small 5 watt, 4" or 6" diameter transceiver is used. The technique is dependent on backscattering from aerosol entrapment by the vortex circulation. Over the altitudes of interest, mostly at 5000 feet, this is not a problem. Such an approach, however, will call for a new instrumentation system aboard an aircraft. However, since such a system can also measure the presence of clear air turbulence in the path of the aircraft, its dual function may justify its application.

By far the cheapest and simplest approach to vortex detection is in the application of passive radiometric techniques. The trailing vortex, with its fluid dynamic, turbulent and spectroscopic signatures does present an interesting measurement medium which is beginning to be exploited. The 8 to 14 micron radiometric measurements performed several miles behind the generating aircraft to detect the presence of water vapor, show great promise. Since water vapor is a major exhaust component of the jet, its detection over long distances is a direct indication of the presence of the vortex. Such a system, however, may not properly operate in cloudy and humid atmospheric environments, since it prefers a dry ambient with respect to the vortex.

The other airborne systems considered, i.e., incoherent Lidar, Raman shift techniques, fluorescence scattering, acoustic radar, ultraviolet emissions or measurement of the heat content of the wake by radiometric techniques, do not possess the prerequisites established

in the X-band or millimetric wave radar, coherent laser Doppler and passive water vapor emission measurement systems. Hence, their further pursuit may not be as useful as the above three approaches.

What is necessary, above all, is a scientific and systems engineering program directed at the detailed measurement of aircraft trailing vortex characteristics in order that through a proper understanding of their physics, the necessary systems can evolve and be shown to be practical.